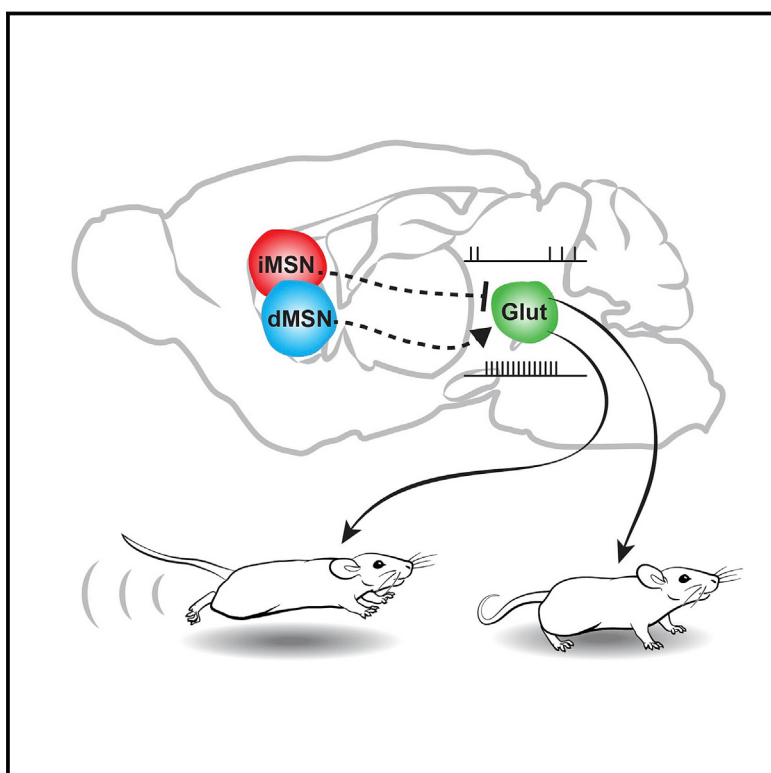


Cell-Type-Specific Control of Brainstem Locomotor Circuits by Basal Ganglia

Graphical Abstract



Authors

Thomas K. Roseberry, A. Moses Lee,
Arnaud L. Lalive, Linda Wilbrecht,
Antonello Bonci, Anatol C. Kreitzer

Correspondence

akreitzer@gladstone.ucsf.edu

In Brief

The basal ganglia bi-directionally regulate a population of brainstem glutamatergic neurons that encode features of running behavior. Cell-type-specific control of functionally distinct neuronal subpopulations may represent a more general principle underlying the regulation of motor behavior by basal ganglia.

Highlights

- Basal ganglion circuits regulate the mesencephalic locomotor region (MLR)
- Basal ganglion output neurons selectively target MLR glutamatergic neurons
- MLR glutamatergic neurons are necessary and sufficient for locomotion
- MLR glutamatergic neurons are required for basal ganglion locomotor control

Cell-Type-Specific Control of Brainstem Locomotor Circuits by Basal Ganglia

Thomas K. Roseberry,^{1,2,9} A. Moses Lee,^{1,2,3,9} Arnaud L. Lalive,¹ Linda Wilbrecht,⁴ Antonello Bonci,^{5,6,7} and Anatol C. Kreitzer^{1,2,3,8,*}

¹The Gladstone Institutes, San Francisco, CA 94158, USA

²Neuroscience Graduate Program, University of California, San Francisco, San Francisco, CA 94158, USA

³Medical Scientist Training Program, University of California, San Francisco, San Francisco, CA 94158, USA

⁴Department of Psychology, University of California, Berkeley, Berkeley, CA 94720, USA

⁵Intramural Research Program, Synaptic Plasticity Section, National Institute for Drug Abuse, Baltimore, MD 21224, USA

⁶Solomon H. Snyder Department of Neuroscience, Johns Hopkins University, Baltimore, MD 21205, USA

⁷Department of Psychiatry, Johns Hopkins University, Baltimore, MD 21287, USA

⁸Departments of Physiology and Neurology, University of California, San Francisco, San Francisco, CA 94158, USA

⁹Co-first author

*Correspondence: akreitzer@gladstone.ucsf.edu

<http://dx.doi.org/10.1016/j.cell.2015.12.037>

SUMMARY

The basal ganglia (BG) are critical for adaptive motor control, but the circuit principles underlying their pathway-specific modulation of target regions are not well understood. Here, we dissect the mechanisms underlying BG direct and indirect pathway-mediated control of the mesencephalic locomotor region (MLR), a brainstem target of BG that is critical for locomotion. We optogenetically dissect the locomotor function of the three neurochemically distinct cell types within the MLR: glutamatergic, GABAergic, and cholinergic neurons. We find that the glutamatergic subpopulation encodes locomotor state and speed, is necessary and sufficient for locomotion, and is selectively innervated by BG. We further show activation and suppression, respectively, of MLR glutamatergic neurons by direct and indirect pathways, which is required for bidirectional control of locomotion by BG circuits. These findings provide a fundamental understanding of how BG can initiate or suppress a motor program through cell-type-specific regulation of neurons linked to specific actions.

INTRODUCTION

The ability to move through the environment to obtain energy, escape predators, and reproduce is fundamental for an animal's survival. In vertebrates, phylogenetically conserved brainstem and spinal circuitry mediates the control of axial muscles and limbs that drive locomotion (Garcia-Rill, 1986; Grillner et al., 2005; Orlovsky et al., 1999; Shik et al., 1966a). In addition, upstream circuitry responsible for deciding when and how to move must be engaged. The basal ganglia (BG) has long been hypothesized to be a key arbitrator of the decision process that results in goal-directed locomotion (Garcia-Rill, 1986; Grill-

ner et al., 2008; Hikosaka et al., 2000). Canonically, the BG consists of two pathways that separate at the level of the striatum, the main input nucleus of the BG. Striatal medium spiny neurons (MSNs) expressing the dopamine D1 receptor mark the direct pathway (dMSNs) and are proposed to facilitate movement, and MSNs expressing the dopamine D2 and adenosine 2a (A2a) receptor mark the indirect pathway (iMSNs) and are proposed to suppress movement (Albin et al., 1989; DeLong, 1990; Kreitzer and Malenka, 2008). These pathways re-converge in the substantia nigra pars reticulata (SNr), the primary output nucleus of basal ganglia in rodents, which provides tonic inhibition of downstream structures responsible for the execution of motor programs (Hikosaka et al., 2000). Recent work from our laboratory has established that optogenetic activation of dMSNs increases locomotion, whereas activation of iMSNs suppresses locomotion (Kravitz et al., 2010). However, the effect of basal ganglia circuitry on downstream targets controlling locomotion remains unknown.

The BG locomotor command is thought to be relayed to spinal cord central pattern generators through the mesencephalic locomotor region (MLR), a brainstem area first described in 1966 by Shik et al. (1966b). The MLR is defined functionally as a mesencephalic region in which increasing intensities of electrical stimulation induce a transition from a stationary state to walking and then running with short latencies (Shik et al., 1966a, 1966b). In mammals, the MLR overlaps with the cuneiform nucleus (Cun), mesencephalic reticular nucleus (MRN), and pedunculopontine tegmental nucleus (PPTg) (Garcia-Rill et al., 1986; Ryczko and Dubuc, 2013). The MLR is comprised of three neurochemically distinct cell types: glutamatergic, GABAergic, and cholinergic (Martinez-Gonzalez et al., 2011). Although the major cell populations of the MLR give rise to ascending projections into the forebrain that may be relevant for reward, arousal, and cortical state (Ehrich et al., 2014; Grace, 2010; Lee et al., 2014; Thompson and Felsen, 2013), the control of locomotion appears to be driven through descending outputs because locomotion is intact in decerebrate animals (Bedford et al., 1992; Whelan, 1996).

Previous work has demonstrated that subsets of neurons in the MLR are correlated with locomotion (Lee et al., 2014; Norton

et al., 2011; Thankachan et al., 2012). However, less is known about the activity of identified MLR glutamate neurons in vivo and whether their activity is actually necessary for locomotion. Moreover, the function of the cholinergic and GABAergic populations during locomotion is not clear. To investigate the locomotor function of MLR cell types and their control by BG circuitry, we combined cell-type-specific optogenetic manipulations, in vivo single-unit recording from identified cells, virus-based circuit mapping, and high-resolution behavioral assays to explore how signals from the BG are transduced into locomotion through the MLR. Our results highlight the functional differences among cell types in the MLR and the remarkable specificity of BG-brain-stem projections. In addition to defining the pathway through which BG regulate locomotion, these results provide a more general framework for how BG can initiate or suppress action by specific modulation of neuronal sub-types associated with a motor program.

RESULTS

Identification of the Mouse MLR

To identify the location of the MLR in the mouse, we used a head-fixed preparation that allowed the subject to walk on a spherical treadmill (trackball) suspended by air (Figure 1A). All subsequent experiments were performed using this preparation unless stated otherwise. Five seconds of electrical stimulation at 20 Hz using a bipolar electrode placed near the PPTg elicited a transition from a stationary state to running (Figures 1B and 1C; mean latency to movement onset, 1580 ± 165 ms), confirming the existence of the MLR. To determine the anatomical extent of the MLR, we systematically stimulated across multiple areas in the mesencephalon and histologically confirmed electrode placements that elicited locomotion with latencies of <2 s. These experiments confirmed that the MLR overlaps with the Cun, PPTg, and MRN (Figure 1D), consistent with other species (Ryczko and Dubuc, 2013).

Bidirectional Modulation of MLR Neurons by the BG

The direct and indirect pathways of the BG exert opposing effects on locomotion (Bateup et al., 2010; Kravitz et al., 2010). To determine how these pathways modulate activity in the MLR, we injected D1-Cre mice to activate dMSNs or A2a-Cre mice to activate iMSNs with an adeno-associated virus for Cre-dependent expression of channelrhodopsin (double-floxed inverted open reading frame [DIO]-ChR2) into the striatum. We then recorded from well isolated, single units in the MLR while stimulating ChR2-expressing neurons in the striatum (Figures 1E and 1I). Unilateral dMSN stimulation resulted in contraversive locomotion when initiated while the mouse was stationary (mean latency to movement onset, 565 ± 78 ms; Figure 1F). Although a majority of MLR neurons increased their firing rate in response to dMSN stimulation, a large fraction was either unmodulated or inhibited (Figures 1F and 1G). We continued to record these neurons after the stimulation session as the mice ran spontaneously on the trackball. Receiver operating characteristic (ROC) analysis revealed that neurons excited by dMSN stimulation were also significantly more predictive of the running state than the stationary state compared with dMSN-unmodulated or dMSN-

inhibited neurons (Figure 1G; $p < 0.01$, Kruskal-Wallis one-way ANOVA, $\chi^2_{2,39} = 15.96$, with Dunn-Sidak post test). Conversely, 5 s of bilateral iMSN stimulation resulted in a transition from running to the stationary state (mean deceleration onset, 651 ± 34 ms) and inhibition of a majority of recorded units in the MLR (Figures 1I and 1J). ROC analysis of spontaneous running revealed no relationship between iMSN modulation and prediction of the locomotor state (Figure 1J). These results demonstrate that the BG can modulate activity within the MLR, although the responses within the MLR are heterogeneous.

Functional Dissection of MLR Cell Types

To better understand the relationship between MLR cell types and locomotion, we next examined how optogenetic activation of each cell type affects locomotion. Glutamatergic or GABAergic neurons were transduced by injecting a Cre-inducible virus expressing ChR2-YFP into vGLUT2-Cre or vGAT-Cre mice (Figures 2B and 2C). Whole-cell recordings confirmed that infected neurons released either glutamate or GABA by blocking excitatory postsynaptic currents (EPSCs) or inhibitory postsynaptic currents (IPSCs), respectively, with antagonists (Figures S1A–S1D). Cholinergic neurons were labeled in transgenic mice expressing ChR2-YFP under the choline acetyltransferase promoter (Zhao et al., 2011; Figure 2A). 10-ms light pulses delivered at 20 Hz to the glutamatergic population for 5 s elicited robust locomotion (Figures 2F and 2I) at significantly shorter latencies than electrical stimulation (mean movement onset, 211 ± 22 ms; $p < 0.01$; Wilcoxon rank-sum test). The speed reached at the end of stimulation was graded by stimulation frequency (Borgius et al., 2010; Lee et al., 2014), a canonical feature of the MLR (Figure 2K). In contrast, stimulation of the GABAergic population during running caused deceleration (mean deceleration onset, 837 ± 99 ms; Figures 2H and S2F) but no change when the mouse was stationary at the beginning of stimulation (Figures 2E and 2J). Choline acetyltransferase (ChAT) neuron stimulation resulted in a significant increase in speed during trials when the mouse was running but not when the mouse was stopped (Figures 2D, 2G, and 2J and S2F). Therefore, ChAT neurons appear to modulate locomotion but are not sufficient to drive locomotion at short latencies. This modulation did not appear to result from co-release of glutamate or GABA because no EPSCs or IPSCs were observed in the MLR during light stimulation in slice (Figure S1E). eYFP controls showed no significant changes in locomotion (Figures 2J and S2F). Together, these results indicate that increased activity within the glutamatergic population alone is sufficient to drive locomotion.

MLR Glutamatergic Neurons Encode Locomotion

To understand how MLR glutamatergic neuron firing relates to locomotion, we injected vGLUT2-Cre mice with DIO-ChR2 in the MLR to optogenetically identify glutamatergic neurons and record their activity during spontaneous locomotion (Figure 3A). Experiments began with an identification session in which 473-nm light was pulsed for 10 ms at 1–2 Hz while evoked single-unit activity was recorded. Well isolated single units that displayed increased firing within 5 ms of light onset and had spontaneous and light-evoked waveform correlations of >0.9 (Pearson's correlation coefficient) were considered

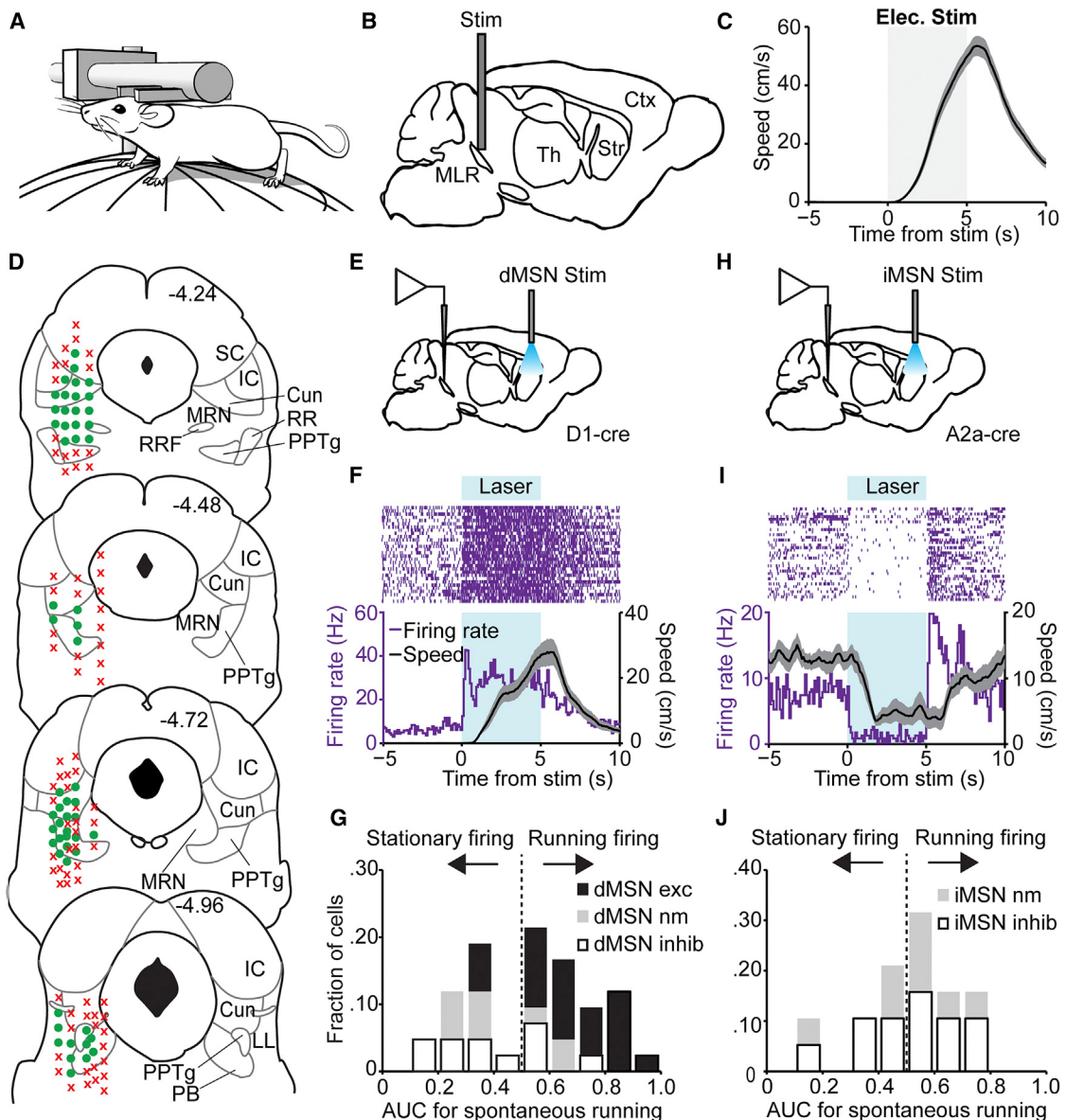


Figure 1. Mapping and Bidirectional BG Regulation of the MLR

(A) Illustration of the head-fixed trackball setup.

(B) Schematic of stimulation within the MLR. Th, thalamus; Str, striatum; Ctx, cortex.

(C) Population time course for mouse speed aligned to 20-Hz electrical stimulation (Elec. stim., n = 7 mice).

(D) MLR mapping using electrical stimulation. Green circles represent electrode placement at which stimulation elicited locomotion (>5 cm/s) with short latency (<2 s), red Xs represent electrode placement where no running was observed. IC, inferior colliculus; RRF, retrorubral field; RR, retrorubral nucleus; LL, lateral lemniscus; PB, parabrachial nucleus (n = 13 mice).

(E) Schematic for stimulation of striatal dMSNs while recording activity in the MLR.

(F) Example neuron excited during dMSN stimulation. Top: rasters of individual trials. Bottom: peristimulus time histogram (PSTH) of firing rate (purple line) and mouse speed (black line) aligned to onset of stimulation.

(G) Histogram of AUCs for speed versus firing rate during a spontaneous locomotor session after dMSN stimulation. Black bars, neurons excited by dMSN stimulation (dMSN exc); gray bars, neurons unmodulated by dMSN stimulation (dMSN nm); open bars, neurons inhibited by dMSN stimulation (dMSN inhib) (n = 42 neurons from 4 mice).

(H) Schematic for stimulation of striatal iMSNs while recording activity in the MLR.

(I) Example neuron inhibited during iMSN stimulation as in (F).

(J) Histogram of AUCs for speed versus firing rate during a spontaneous locomotor session after iMSN stimulation. Gray bars, neurons unmodulated by iMSN stimulation (iMSN nm); open bars, neurons inhibited by iMSN stimulation (iMSN inhib) (n = 26 neurons from 4 mice). All shaded regions, SEM.

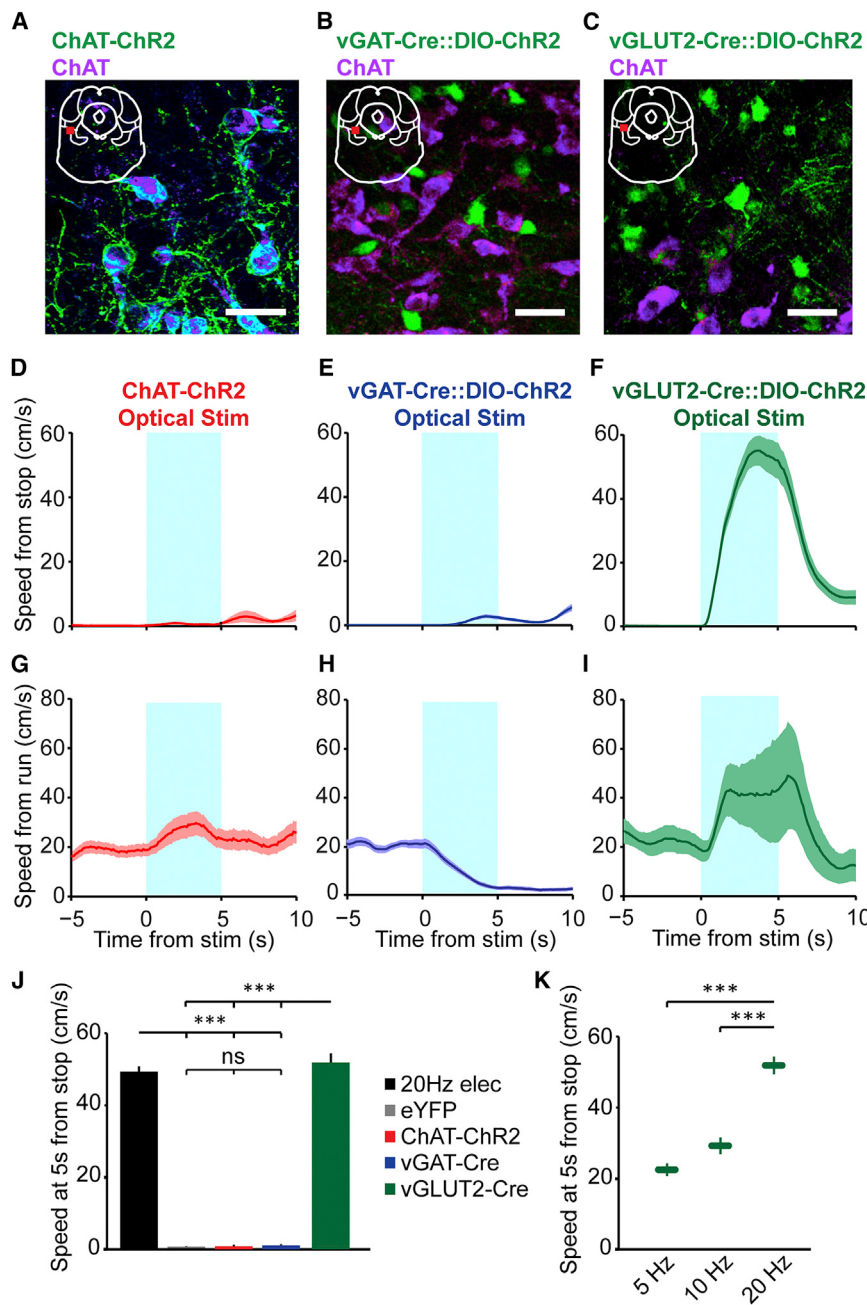


Figure 2. Distinct Functions of MLR Cell Types

(A–C) Confocal images of coronal sections through the MLR of ChAT-ChR2 (A), vGAT-Cre::DIO-ChR2 (B), and vGLUT2-Cre::DIO-ChR2 (C) counterstained for ChAT, which demarcates the boundaries of the PPTg. Insets show the location of the image. Scale bars, 25 μ m.

(D–I) Population time course for mouse speed aligned to 20-Hz optical stimulation from stationary (D–F) and running (G–I) states in ChAT-ChR2 mice (D and G; n = 5 mice, 7 hemispheres), vGAT-Cre::DIO-ChR2 mice (E and H; n = 4 mice, 6 hemispheres), and vGLUT2-Cre::DIO-ChR2 mice (F and I; n = 6 mice, 7 hemispheres). Shaded regions, SEM.

(J) Summary of population speed 5 s after stimulation onset (**p < 10⁻⁴, Kruskal-Wallis one-way ANOVA, $\chi^2_{3,243} = 175.52$, p < 10⁻¹⁰, with Dunn-Sidak post test). ns, not significant.

(K) Summary of speed at 5 s during graded stimulation of glutamatergic neurons (**p < 10⁻⁴, Kruskal-Wallis one-way ANOVA, $\chi^2_{2,167} = 175.52$, p < 10⁻⁵, with Dunn-Sidak post test). All shaded regions, SEM.

See also Figures S1 and S2.

glutamatergic (Figures 3B–3D). A locomotor session followed in which the same single-unit activity was recorded during spontaneous running (Figure 3E). A second identification session was run after the locomotor session to ensure that there was no drift. Neurons that were held for all three sessions (based on cluster analysis, see Experimental Procedures) and found to be inside the functional boundaries of the MLR were kept for analysis (Figures 3B–3D). To quantify how closely these neurons encode the running state, we performed ROC analysis on the firing rate and speed data. The firing rate of individual MLR glutamatergic neurons was highly predictive of the running state (Figure 3F).

In contrast, unidentified neurons from a separate cohort of mice displayed significantly lower areas under the curve (AUCs), indicating functional heterogeneity among MLR neuronal subpopulations (Figure 3F). To further dissect this result, we tested the locomotor-predictive MLR glutamatergic neurons for correlations with speed using a linear regression model. This analysis yielded two distinct populations: one that predicts locomotor state alone and one that predicts state and correlates with speed (Figure 3G). We next tested whether the glutamatergic neuron firing rate was predictive of locomotor starts. Glutamatergic neurons as a population increased their firing rate prior to the onset of a spontaneous locomotor start (Figure 3H). However, in individual trials, spiking increase onset was highly variable, and an absolute threshold at which spiking would correlate with running onset was not observed (Figure 3H, inset). Therefore, we tested the prediction that spiking increases during the stationary state would result in an increased probability of running onset. Indeed, an increased firing rate during the stationary state was correlated with an increase in the probability of a start occurring within the next second (Figure 3I; Pearson's correlation coefficient; p < 0.01). This suggests that, at the individual level, glutamatergic neurons do not predict the timing of locomotion onset. Rather, these neurons contribute to an increased probability of locomotion that is read out from the population. These findings indicate

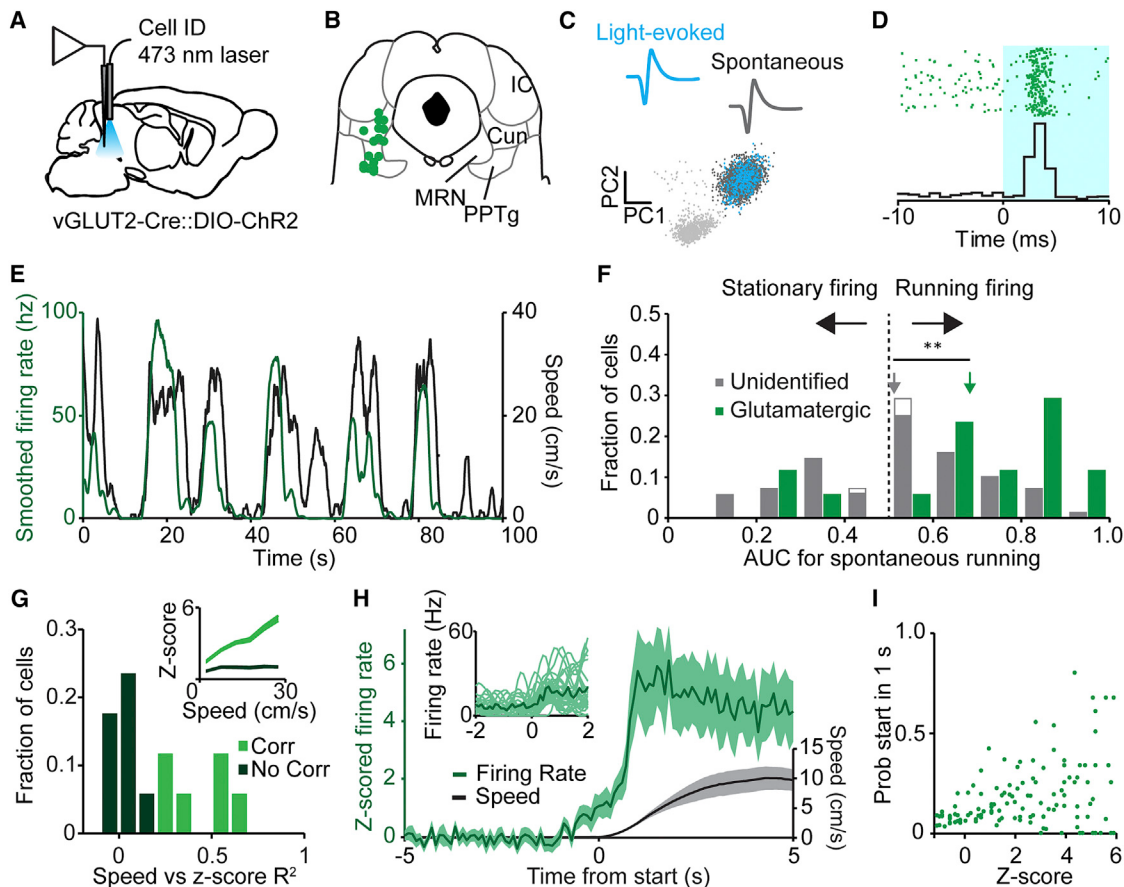


Figure 3. Characterization of MLR Glutamatergic Neurons

- (A) Schematic of the optical tagging and recording setup in vGLUT2-Cre::DIO-ChR2 mice. ID, identified.
 - (B) Recording sites for ChR2-positive (glutamatergic) neurons.
 - (C) Top: light-evoked and spontaneous waveforms of an identified neuron. Bottom: PC1 versus PC2 for the neuron. Light gray dots, noise; dark gray dots, spontaneous spikes; blue dots, light-evoked spikes.
 - (D) Raster (top) and PSTH (bottom) for a light-reactive neuron showing 3-ms latency aligned to laser onset.
 - (E) Smoothed firing rate of the neuron identified in (C) and (D) (green line, left axis) plotted with the speed of the mouse (black line, right axis).
 - (F) Histogram of AUCs for all recorded neurons during spontaneous locomotion. Green bars, identified glutamatergic neurons (all significantly encoded the stationary or locomotor state); filled gray bars, unidentified neurons recorded in the MLR from a separate cohort that significantly encoded the stationary or running state; open gray bars, neurons that did not significantly encode either state; arrows, means ($^{**}p < 0.001$, Wilcoxon rank-sum test).
 - (G) Histogram of R^2 values for the glutamatergic neurons that predicted locomotion in (F) ($n = 14$). Light green bars, speed-correlated (corr) neurons; dark green bars, neurons not correlated with speed.
 - (H) Population Z-scored firing rate of identified glutamatergic neurons (green trace) aligned to onset of locomotion. Black trace, speed. Inset, individual example firing rate traces (light green) and average (dark green) aligned to starts.
 - (I) Probability of a start within 1 s given Z-scored firing rate. Each point represents one binned data point (0.1-SD bins) from one neuron.
- All shaded regions, SEM. See also Figure S3.

that MLR glutamatergic activity is tightly linked with and predictive of an animal's locomotor state and speed.

MLR Glutamatergic Neurons Are Required for Spontaneous Locomotion

Because activity in MLR glutamatergic neurons is sufficient for locomotion and encodes locomotor state and speed, we next tested whether they are necessary for spontaneous running. Previous experiments examining inhibition of the MLR have reported mixed effects on locomotion, most likely because of the long-term and non-specific effects of pharmacological interventions

(Saper et al., 1979; Sinnamon et al., 1987). To specifically inhibit the glutamatergic population on a millisecond timescale, we expressed halorhodopsin (eNpHR3.0) under the calcium/calmodulin-dependent kinase II α (CaMKII α) promoter, which targets glutamatergic neurons in the MLR with high selectivity (Lee et al., 2014; Figures 4A and S3A and S3B). Photo-inhibition of MLR glutamatergic neurons caused running animals to decelerate rapidly, often to a full stop (mean deceleration onset, 835 ± 103 ms; Figures 4B–4D), whereas control animals showed only a gradual decrease in mean speed over time, consistent with a low baseline probability of spontaneous stopping. This

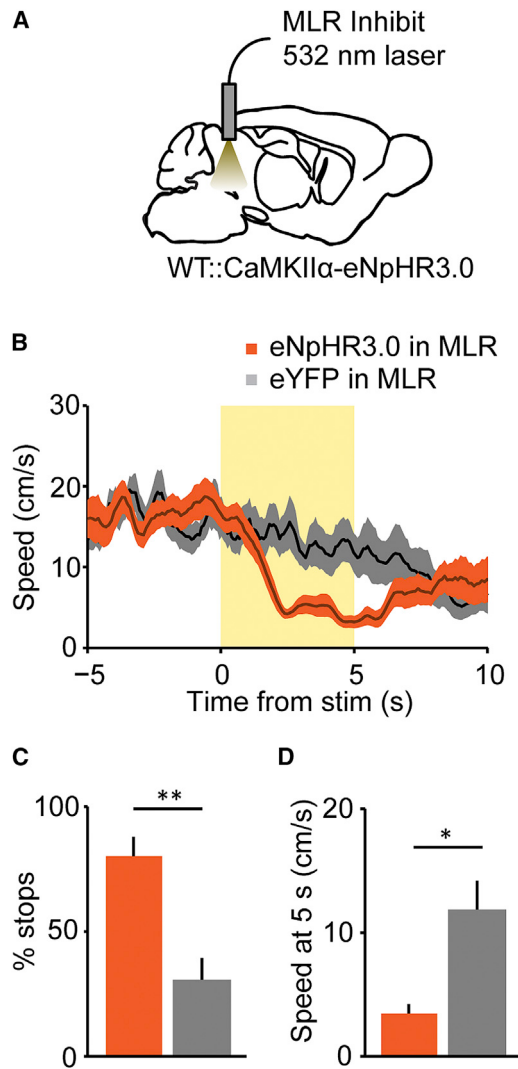


Figure 4. Inhibition of MLR Glutamatergic Neurons Impedes Running

(A) Experimental schematic for inhibiting glutamatergic neurons in the MLR. WT, wild-type.
 (B) Speed aligned to laser onset or with no stimulation (eNpHR3.0 in MLR, orange line, n = 4 mice; eYFP in MLR, black line, n = 6 mice).
 (C) Number of stops during laser inhibition for each group.
 (D) Speed summary data 5 s after onset of laser inhibition.

*p < 0.05, **p < 0.01, Wilcoxon rank-sum test. Shaded regions, SEM.

result indicates that MLR glutamatergic neurons are necessary for spontaneous locomotion.

MLR GABAergic Neurons Suppress Activity in the MLR

Because activation of the MLR GABAergic population decreased locomotion, we next examined whether these neurons locally inhibited other MLR neurons. In MLR slices prepared from mice expressing ChR2-eYFP in GABAergic neurons, IPSCs and inhibition of spiking were observed during whole-cell recordings from ChR2-eYFP-negative cells in response to optogenetic stimulation (Figures S1C–S1DD and S4A). In vivo re-

cordings during optogenetic stimulation of MLR GABA neurons demonstrated that the majority of non-light-sensitive neurons were inhibited for the duration of illumination (Figures S4B–S4C). Because activity in MLR glutamatergic neurons is required for running (Figure 4), deceleration and stopping because of optogenetic activation of GABAergic neurons is likely in part due to local inhibition of MLR glutamatergic neurons. However, in vivo recordings from optogenetically identified MLR GABA neurons during spontaneous locomotion revealed heterogeneous responses, indicating additional complexity in the composition and function of this subpopulation (Figure S4D).

Brain-wide Tracing of Monosynaptic Inputs to MLR Glutamatergic and GABAergic Neurons

We next tested the connection strength between the BG and the two MLR populations displaying the most robust effects on locomotion. In theory, BG-driven locomotion could be initiated by disinhibition of MLR glutamatergic neurons (Grillner et al., 2008; Hikosaka et al., 2000) or inhibition of GABAergic neurons. A difference in connection strength from the BG could discriminate between these possibilities. We used a cell-type-specific G-deleted rabies virus strategy to map neurons that directly target MLR glutamatergic or GABAergic neurons (Wall et al., 2013). vGLUT2-Cre or vGAT-Cre mice were injected with an adeno-associated virus (AAV) encoding rabies virus glycoprotein (RG) and a separate virus encoding a Cre-inducible avian receptor (TVA-mCherry) in the MLR on day 1. Only Cre-expressing cells will express the avian tumor virus receptor A (TVA receptor), which is required for rabies transduction. On day 14, mice were injected in the same area with modified rabies virus. Nine days later, the mice were perfused, and the brains were processed (Figure 5A). Retrograde trans-synaptic labeling from MLR glutamatergic neurons revealed dense projections from several BG nuclei, whereas few, if any, projections targeted MLR GABAergic neurons (Figures 5C–5F). A brain-wide survey of long-range projections to these cell types revealed another strong projection to MLR glutamatergic neurons from the central amygdala and oval bed nucleus of the stria terminalis (ovBNST), GABAergic nuclei that could play a role in fear- and anxiety-associated behaviors such as freezing (Figure 5F; LeDoux, 2000). Major MLR GABAergic targeting regions included the superior colliculus, dorsal raphe, laterodorsal tegmentum, and ovBNST. Together, these results suggest a specific role for MLR glutamatergic neurons in the control of locomotion by upstream targets and, notably, the BG.

Modulation of MLR Glutamatergic Neurons Is Required for Bidirectional Control of Locomotion by BG Circuitry

To test how the direct and indirect pathways specifically modulate the MLR glutamatergic population, we optogenetically identified MLR glutamatergic neurons and recorded their activity while simultaneously stimulating dMSNs or iMSNs in the striatum. We expressed ChR2 in dMSNs or iMSNs using Cre-dependent viruses injected into the striatum of D1- or A2A-Cre mice. In the same mice, we expressed ChR2 in MLR glutamatergic neurons for optogenetic identification using a virus expressing ChR2 under the CaMKII α promoter (Figures 6A and 6E). Each

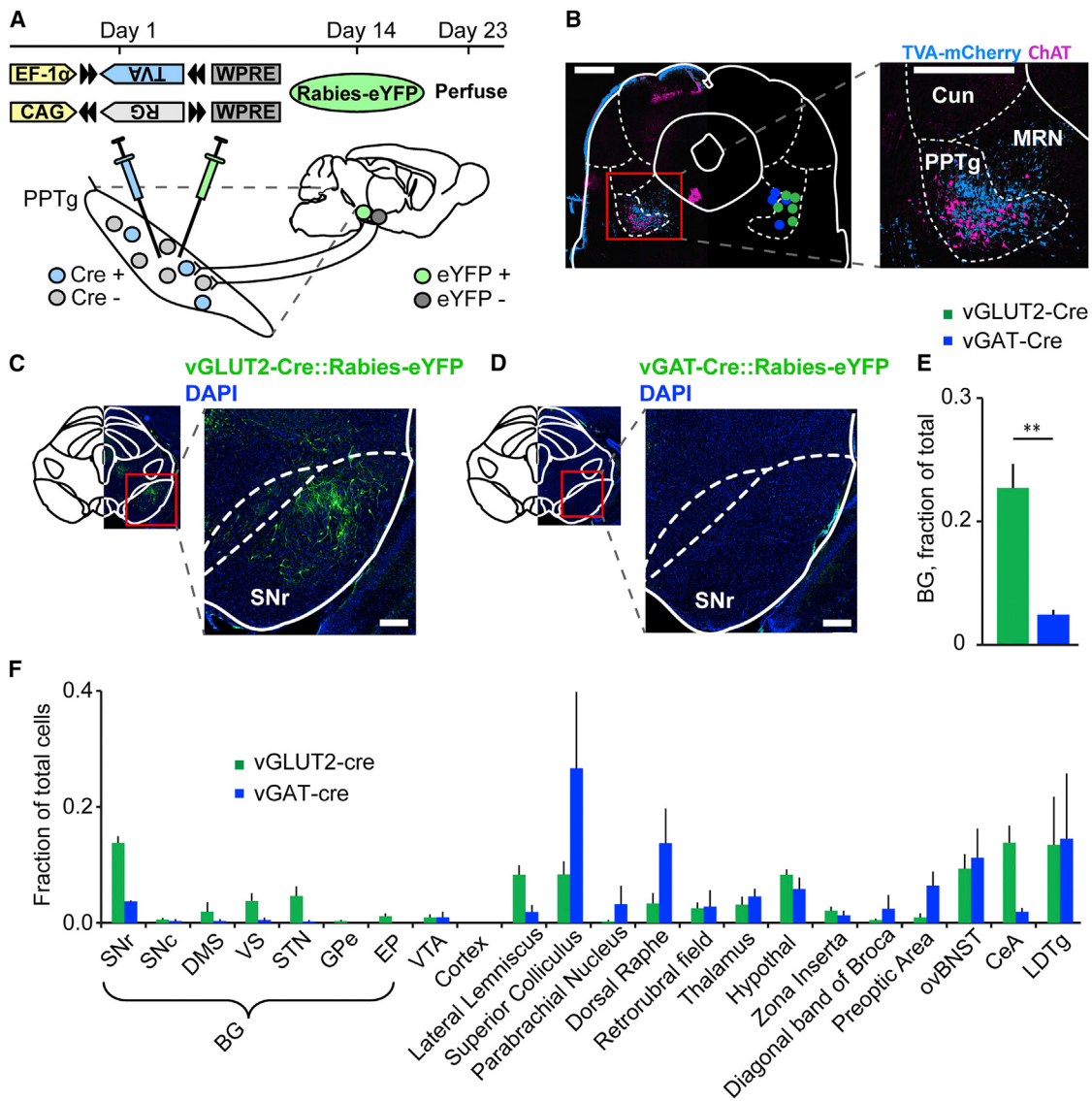


Figure 5. Brain-wide Mapping of Inputs to MLR Glutamatergic and GABAergic Neurons

(A) Schematic and time course of the experiment.

(B) Left: coronal section through the MLR showing TVA-mCherry labeling (blue) around the PPTg (labeled with ChAT staining, pink) and center of mass of TVA and RG injection sites (blue dots, vGAT-Cre::TVA+RG; green dots, vGLUT2-Cre::TVA+RG). Right: close-up of infected cells. Scale bars, 500 μ m.

(C and D) Examples of eYFP expression in the SNr in vGLUT2-Cre::Rabies-eYFP (C) and vGAT-Cre::Rabies-eYFP (D) mice. Scale bars, 200 μ m.

(E) Quantification of labeled cell counts from all BG nuclei in vGLUT2-Cre::Rabies-eYFP (green bars) and vGAT-Cre::Rabies-eYFP mice (blue bars). ** $p < 0.01$, Wilcoxon rank-sum test.

(F) Quantification of ipsilateral inputs to MLR glutamatergic (green) and GABAergic (blue) neurons. SNC, substantia nigra pars compacta; DMS, dorsomedial striatum; VS, ventral striatum; VTA, ventral tegmental area; CeA, central amygdalar nucleus; LDTg, laterodorsal tegmental nucleus. Error bars, SEM.

experiment began with an identification session to find putative glutamatergic neurons based on the criteria listed previously. CaMKII α -ChR2 had similar light responses as the vGLUT2-Cre::DIO-ChR2 strategy (Figures S3C–S3D). After MLR neuron identification, we stimulated striatal dMSNs or iMSNs (5 s of continuous light) while recording MLR glutamatergic neuron activity. This was followed by a second MLR neuron identification session. Fiber and electrode placements were confirmed post hoc (Figures S5A–S5F).

Unilateral dMSN stimulation significantly increased the firing rate in 25 of 26 identified MLR glutamatergic neurons (Figure 6B). In each case, the increase in firing rate preceded movement onset (mean latency to excitation, 176 \pm 18 ms; Figures 6B and S5J–S5K). In contrast, bilateral iMSN stimulation delivered while the mouse was running significantly decreased the firing rate in 25 of 27 identified MLR glutamatergic neurons (Figure 6F). Deceleration was preceded by a decrease in firing rate in the majority of identified MLR glutamatergic neurons (mean latency

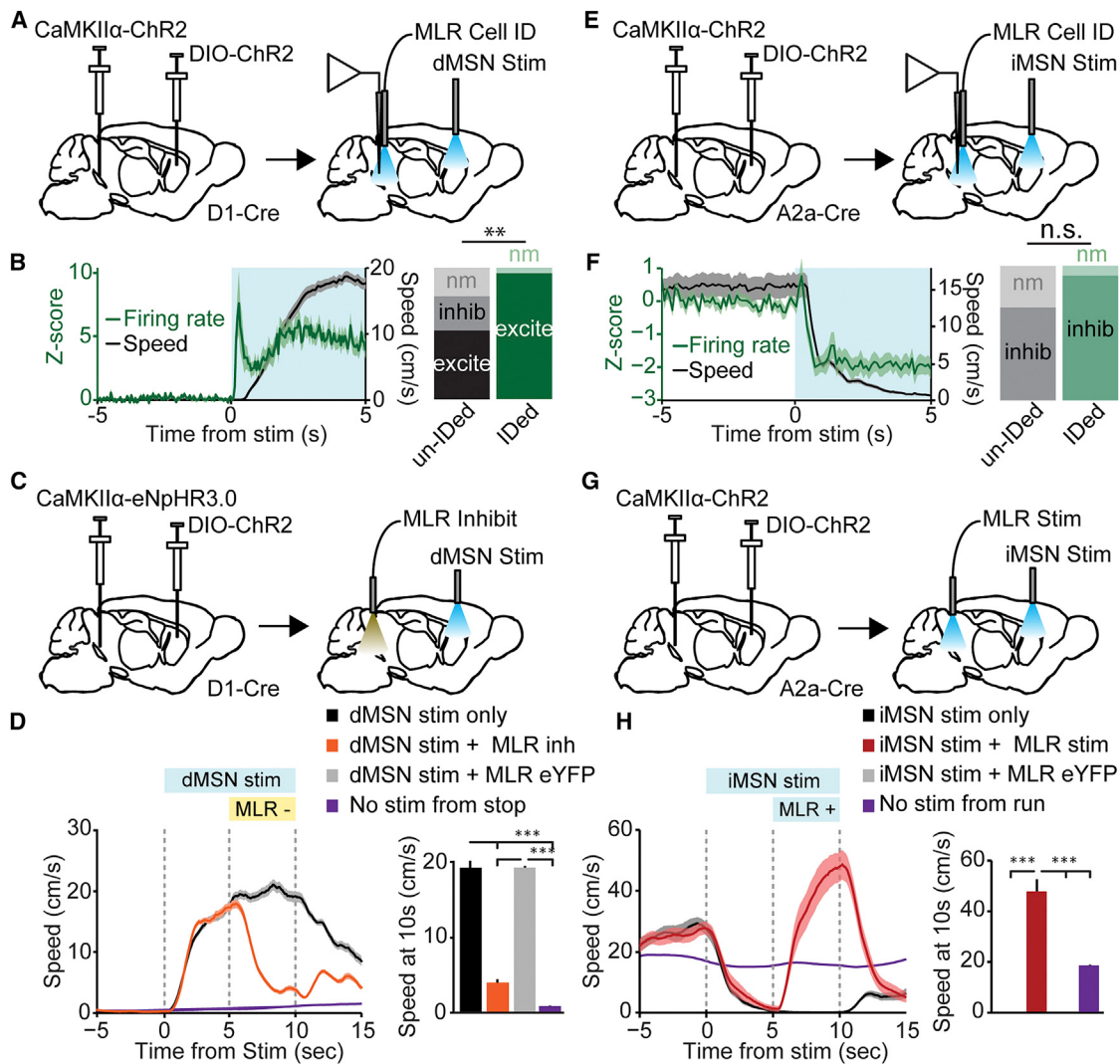


Figure 6. MLR Glutamatergic Neurons Are Necessary and Sufficient to Reverse the Effects of BG Stimulation

(A) Schematic for recording MLR glutamatergic neurons while activating dMSNs in the striatum.

(B) Left: Z-scored firing rate of identified glutamatergic neurons (green line, left axis) and speed (black line, right axis) aligned to onset of 5-s unilateral dMSN stimulation from stop. Right: fractions of excited (excite), inhibited (inhib), or non-modulated (nm) units in unidentified recordings (un-IDed, left) and in identified glutamatergic cells (IDed, right) (identified: 25 excited, 0 inhibited, 1 non-modulated from 4 mice; unidentified: 22 excited, 11 inhibited, 9 non-modulated from 4 mice; **p < 0.001, χ^2 test).

(C) Schematic for stimulating dMSNs in the striatum while inhibiting MLR glutamatergic neurons.

(D) Left: speed aligned to unilateral dMSN stimulation. Orange line, trials in which green light was turned on in the MLR 5 s after dMSN stimulation; black line, interleaved trials in which green light was omitted; purple line, no stimulation trials when mouse was stopped. Right: speed 10 s after onset of dMSN stimulation (**p < 10⁻⁴, Kruskal-Wallis one-way ANOVA, $\chi^2_{3,136} = 92.35$, p < 10⁻¹⁰, with Dunn-Sidak post test).

(E) Schematic for recording identified MLR glutamatergic neurons while activating iMSNs in the striatum.

(F) Left: Z-scored firing rate of identified glutamatergic neurons (green line, left axis) and speed (black line, right axis) aligned to onset of 5-s bilateral iMSN stimulation from running. Right: summaries for the number of inhibited or non-modulated units in unidentified (left) recordings and identified (right) glutamatergic neurons (identified: 25 inhibited, 2 unmodulated from 4 mice; unidentified: 18 inhibited, 8 unmodulated from 3 mice; p = 0.09, χ^2 test).

(G) Schematic for stimulating iMSNs in the striatum while stimulating glutamatergic cells in the MLR.

(H) Left: time course of mouse speed aligned to bilateral iMSN stimulation. Red line, trials in which blue light was turned on in the MLR at 20 Hz 5 s after iMSN stimulation; black line, interleaved trials in which green light was omitted; purple line, no stimulation trials when the mouse was running. Right: summary of mouse speed 10 s after onset of iMSN stimulation (**p < 10⁻⁴, Kruskal-Wallis one-way ANOVA, $\chi^2_{3,105} = 75.06$, p < 10⁻¹⁰, with Dunn-Sidak post test).

Shaded regions, SEM. See also Figures S5 and S6.

to inhibition, 460 ± 48 ms; Figures 6F and S5H–S5I). To better compare dMSN and iMSN stimulation latencies (Freeze et al., 2013; Oldenburg and Sabatini, 2015) we analyzed trials in which

the mouse was stationary prior to iMSN stimulation. Latencies to inhibition were markedly shorter relative to running trials (latency to inhibition, 276 ± 30 ms; Figure S5G) but still longer than

excitation during dMSN stimulation. Finally, in contrast to data obtained from identified glutamatergic neurons, unidentified MLR neurons displayed significantly more heterogeneous responses to stimulation of either pathway (Figures 6B and 6F), indicating that more complex circuit dynamics are controlling the activity of other neuronal subpopulations in the MLR.

Given that MLR glutamatergic neurons are sufficient for locomotion, correlated with locomotion, and modulated by the BG, we next asked whether they are necessary for BG-driven locomotion. To investigate this, we expressed eNpHR3.0 in the MLR under the CaMKII α promoter and ChR2 in dMSNs using a Cre-dependent virus injected into the striatum of D1-Cre mice (Figures 6D and S5E–S5F). Unilateral activation of dMSNs for 10 s elicited locomotion throughout the duration of the stimulation (Figure 6D). During interleaved trials, MLR glutamatergic neurons were optogenetically inhibited from 5–10 s after the onset of dMSN stimulation, which led to a striking decrease in running speed despite continued activation of dMSNs (Figure 6D). As a control, we looked at 1,000 time points when the mouse had been stationary for the same amount of time as “dMSN stim only” and “dMSN stim + MLR inhibition” trials and found that this similar baseline resulted in a spontaneous speed trajectory that did not resemble either stimulation condition. No change in locomotion was observed in trials without MLR inhibition or when light was delivered to MLR glutamatergic neurons expressing only YFP. Qualitatively similar results were observed in freely moving mice (Figure S6).

We then tested whether inhibition of MLR neurons was necessary for locomotor suppression observed with iMSN stimulation. In these experiments, we expressed ChR2 in the MLR under the CaMKII α promoter and ChR2 in iMSNs using a Cre-dependent virus injected into the striatum of A2a-Cre mice (Figures 6G and S5A–S5B). Bilateral activation of iMSNs for 10 s induced locomotor suppression throughout the duration of the stimulation (Figure 6H). This arrest was completely reversed by 20-Hz optical stimulation of MLR glutamatergic neurons delivered 5 s after the onset of the 10-s iMSN stimulation (Figure 6H). This reversal was not observed in eYFP controls. In addition, control trials with similar baselines but no stimulation of the iMSN or MLR glutamatergic neurons showed no changes in running speed. Taken together, these results demonstrate that bidirectional control of locomotion by basal ganglia circuitry requires modulation of MLR glutamatergic neurons.

DISCUSSION

Cell-Type-Specific Control of Locomotion by MLR Neurons

Previous work has shown that the MLR has robust descending projections to the gigantocellular nucleus (Martinez-Gonzalez et al., 2014; Mitani et al., 1988; Rye et al., 1988), also referred to as the ventromedial medulla (Sherman et al., 2015; Skinner et al., 1990). In addition, MLR axons and terminals have been found in the pontine reticular formation (Takakusaki et al., 1996) and nucleus pontine oralis (Garcia-Rill et al., 2001). Collectively, these nuclei form the origin of reticulospinal tracts that project into the spinal cord and mediate various aspects of posture and movement. There may also be spinally projecting

glutamatergic neurons within the boundaries of the MLR (Sherman et al., 2015). Indeed, lesions of the major non-spinal targets of the MLR do not reduce the gross aspects of locomotor function (Noga et al., 1988; Sherman et al., 2015), raising the possibility that the MLR acts as a comprehensive coordinator of locomotion.

Our optogenetic dissection of MLR cell types revealed that only the glutamatergic population was sufficient to elicit running at short latencies, consistent with the classical definition of the MLR (Grillner et al., 2008; Ryczko and Dubuc, 2013; Shik et al., 1966b). This is in agreement with a recent study showing that cells targeted with a CaMKII α -ChR2 virus in the MLR could elicit running (Lee et al., 2014) and consistent with current hypotheses about brainstem locomotor control (Grillner et al., 2005; Sherman et al., 2015). In spite of previous experiments that were unable to stop locomotion via pharmacologic inhibition or lesion of the MLR (Saper et al., 1979; Sinnamon et al., 1987), rapid optogenetic suppression of the MLR glutamatergic population revealed that these neurons are indeed necessary for locomotion.

In contrast to glutamatergic neurons, the MLR GABAergic population caused cessation of locomotion. Although this population encoded both running and stationary states (Figure S4), the deceleration and stopping observed during stimulation could be in part due to local inhibition of the MLR glutamatergic population. However, inhibition of downstream targets is also a possibility. MLR GABA neurons received dense input from limbic centers (amygdala, periaqueductal gray [PAG] and BNST), suggesting that they could be involved in fear-related behavior. GABAergic neurons in neighboring regions have also been shown to suppress locomotion (Giber et al., 2015; Shang et al., 2015), suggesting that GABAergic cells at this level of the mesencephalon share similar functions.

Finally, stimulation of the MLR cholinergic population demonstrated that, although these neurons can modulate locomotion, they are insufficient to initiate it with short latency. This population has been hypothesized previously to control locomotion (Skinner et al., 1990). PPTg cholinergic neurons send projections to the ventromedial medulla, depolarizing glutamatergic cells that, in turn, project to reticulospinal neurons (Brudzynski et al., 1988; Mamiya et al., 2005; Smetana et al., 2010). However, other work has shown that these neurons play a major role in gating the brain state as part of the ascending reticular activating system (Mena-Segovia et al., 2008; Van Dort et al., 2015). Because locomotion and brain state are clearly linked (Lee et al., 2014; Niell and Stryker, 2010), the time course of behavioral changes is critical to consider.

Non-canonical Projections from the BG and Other Nuclei

The BG interface strongly with the MLR, making reciprocal connections from most of its nuclei (Martinez-Gonzalez et al., 2011; Mena-Segovia et al., 2004). Our rabies tracing showed that it is the glutamatergic population—and not the GABAergic population—that is the primary target of these BG connections. In addition, our tracing highlighted a number of non-canonical pathways to the MLR from the BG (entopeduncular nucleus [EP], external globus pallidus [GPe], subthalamic nucleus [STN]) to MLR glutamatergic neurons. The STN projection is of interest because it is predicted to arrive in the MLR prior to the classical

indirect pathway signal through the SNr, and it should drive activity in the opposite direction. Indeed, a small minority of cells displayed a small uptick in firing rate prior to inhibition (Figure 6F), consistent with the idea that this pathway modulates MLR activity, perhaps as a brief arousal signal prior to suppression of locomotion.

Striatal neurons also send projections directly to MLR glutamate neurons. Interestingly, the PPTg, one of the MLR nuclei, also sends projections back to the striatum (Wall et al., 2013) thus forming a reciprocal connection. As iMSNs do not project past the GPe, it is most likely the dMSN population that sends axons to the MLR. As this connection is GABAergic, these cells may form synapses onto the small number of glutamatergic neurons that fire most during the stationary state. dMSNs in the DMS could therefore coordinate the initiation of locomotion by directly inhibiting these cells.

Comparison with Other BG Targets

The BG output nuclei also project to the thalamus and superior colliculus (SC) (Bosch-Bouju et al., 2013; Hikosaka et al., 2000), enabling broad control of cortical and brainstem circuitry. Recent work has shown that direct and indirect pathway stimulation increases and decreases firing rates in the motor cortex, respectively, along with increasing and decreasing lever press frequency in an operant task (Oldenburg and Sabatini, 2015). However, the principles underlying BG control of the thalamus and cortex remain largely mysterious (Bosch-Bouju et al., 2013; Goldberg et al., 2013). In contrast, BG have long been proposed to act as a “gate” for motor behaviors originating from the SC, such as turning and saccades (Girard and Berthoz, 2005; Hikosaka et al., 2000), because the SNr is known to exert tonic inhibitory control over the SC (Chevalier et al., 1984). To initiate an orienting movement, SNr inhibition to the contralateral SC is released, allowing input from the cortex to excite SC neurons, which, in turn, drive the action (Hikosaka and Wurtz, 1983). The SC is topographically organized by the visual field (Schiller and Stryker, 1972), as are SNr inputs (Hikosaka and Wurtz, 1983). Because of this association, BG have been hypothesized to play a role in deciding important targets for orienting (Hikosaka et al., 2006). Between this SC-mediated orienting and MLR-mediated running, these brainstem BG targets are fully capable of defining locomotor trajectories, consistent with decortication studies (Bjurstén et al., 1976). In addition, our rabies result demonstrates that the SC connects directly with the MLR, consistent with previous studies (Martinez-Gonzalez et al., 2011; Perkins et al., 2014; Redgrave et al., 1987), providing another connection through which BG-brainstem connections could exert navigational control.

BG Pathway-Specific Selection and Suppression of Action

Our cell-type-specific recordings from the MLR during iMSN and dMSN stimulation reveal a remarkable degree of homogeneity in the glutamatergic population response. The majority of responses preceded changes in locomotion, suggesting that they were causally related to behavior. In support of this, inhibition of the glutamatergic population during dMSN-induced locomotion caused the mouse to stop running. Although the functional re-

sponses observed in the SNr in response to striatal stimulation are complex (Freeze et al., 2013), the signal becomes surprisingly uniform at the level of the MLR glutamatergic population. Together with the rabies results, this indicates a highly specific connection between BG and locomotor-encoding MLR neurons.

Given its ability to drive a robust behavioral output, the MLR represents an ideal system for understanding the BG role in action selection. Classical models of BG suggest that movement occurs when the direct pathway is active and cessation of movement occurs with indirect pathway activation. However, both pathways appear to be co-active during normal movement (Cui et al., 2013). One possibility is that different information is encoded in the direct and indirect pathway circuits, which, together, form the basis for action selection. For example, indirect pathway activity could encode information about competing behavioral choices. Our data suggest that the balance of activity between the direct and indirect pathways is represented in the firing rate of glutamatergic MLR neurons, which is predictive of the initiation of running and sufficient to drive graded locomotion. Further experiments can help clarify the validity of this model for the MLR and other BG output structures.

EXPERIMENTAL PROCEDURES

Subjects

86 adult transgenic or wild-type mice on a C57BL/6 background aged 50–100 days were used in the experiments. vGLUT2-Cre (The Jackson Laboratory, stock no. 016963), vGAT-Cre (The Jackson Laboratory, stock no. 016962), ChAT-ChR2 (The Jackson Laboratory, stock no. 014546), and wild-type C57BL/6 (The Jackson Laboratory, stock no. 000664) mice were used for optogenetic stimulation, inhibition, or recording experiments. vGLUT2-Cre and vGAT-Cre mice were used for rabies tracing experiments. D1-Cre mice (GENSAT, catalog no. 030778-UCD) were used for dMSN stimulation while recording responses from identified glutamatergic neurons or inhibiting the MLR. A2a-Cre mice (GENSAT, catalog no. 031168-UCD) were used for iMSN stimulation while recording identified responses from identified glutamatergic neurons or stimulating the MLR. vGLUT2-Cre mice crossed into an AI14 line (The Jackson Laboratory, stock no. 007914) were used for confirmation of CAMKII α expression in vGLUT2-expressing neurons. All procedures were in accordance with protocols approved by the University of California, San Francisco Institutional Animal Care and Use Committee.

Surgery

For dMSN or iMSN activation, AAV5-EF1 α -DIO-ChR2-eYFP (University of Pennsylvania) was injected into the dorsomedial striatum at (0.8 mm anterior/posterior axis [AP]/−2.5 dorsal/ventral axis [DV]/± 1.5 medial/lateral axis [ML]) measured from the bregma. For activation of cells in the MLR, AAV5-EF1 α -DIO-ChR2-eYFP or AAV5-CAMKII α -ChR2-eYFP (for glutamatergic neurons) was injected at (−0.8 mm AP/−3.6 DV/± 1.2 ML), measured from the lambda. Where appropriate, fiberoptic ferrules were implanted 0.5 mm above the injection sites. The virus was allowed to express for 2–6 weeks, after which the mice were implanted with a custom-built stainless steel headbar for head fixation. 7–10 days later, the mice were habituated to the trackball until able to run normally, at which point recordings took place.

Recording and Optogenetics

Extracellular recordings were performed using a Plexon data acquisition system (Plexon). A blue laser (473 nm, 100 mW, OEM) was triggered through a transistor-transistor logic [TTL] pulse generator (PulseBlaster, SpinCore Technologies). Trackball velocity was monitored via two optical handheld pointing devices (computer mice) that were connected to the recording computer.

Custom MATLAB (MathWorks) data acquisition software was used to transform optical mouse data packets into speed and time data.

Data Analyses

Data analyses were carried out using built-in (NeuroExplorer, Plexon) and custom-built software in MATLAB (MathWorks). Single units were sorted into clusters using commercially available software (Plexon Offline Sorter 2.4, Plexon). See the [Supplemental Experimental Procedures](#) for further details.

SUPPLEMENTAL INFORMATION

Supplemental Information includes Supplemental Experimental Procedures and six figures and can be found with this article online at <http://dx.doi.org/10.1016/j.cell.2015.12.037>.

AUTHOR CONTRIBUTIONS

A.M.L. conceptualized and initiated the project in the laboratory of A.B., continued the project in the laboratory of L.W., and brought the project to the laboratory of A.C.K., where he conducted experiments together with T.K.R. and co-wrote the manuscript. T.K.R. performed experiments, analyzed all data, and co-wrote the manuscript. A.L.L. performed slice electrophysiology recordings. A.C.K. designed experiments, supervised the project, and co-wrote the manuscript.

ACKNOWLEDGMENTS

We thank Delanie Schulte for assistance with genotyping, histology, and microscopy and the A.C.K. laboratory for comments on the manuscript. This work was funded by NIH R01 NS064984 and P01 DA010154 (to A.C.K.), F31 NS092253 (to T.K.R.), 5T32GM007618-38 (to A.M.L.), RR018928 (to the Gladstone Institutes), a grant from the Swiss National Science Foundation (to A.L.L.), funds from the State of California (to L.W.), and an NIDA intramural program (to A.B.).

Received: September 9, 2015

Revised: October 27, 2015

Accepted: December 22, 2015

Published: January 28, 2016

REFERENCES

- Albin, R.L., Young, A.B., and Penney, J.B. (1989). The functional anatomy of basal ganglia disorders. *Trends Neurosci.* 12, 366–375.
- Bateup, H.S., Santini, E., Shen, W., Birnbaum, S., Valjent, E., Surmeier, D.J., Fisone, G., Nestler, E.J., and Greengard, P. (2010). Distinct subclasses of medium spiny neurons differentially regulate striatal motor behaviors. *Proc. Natl. Acad. Sci. USA* 107, 14845–14850.
- Bedford, T.G., Loi, P.K., and Crandall, C.C. (1992). A model of dynamic exercise: the decerebrate rat locomotor preparation. *J. Appl. Physiol.* 72, 121–127.
- Bjursten, L.M., Norrsell, K., and Norrsell, U. (1976). Behavioural repertory of cats without cerebral cortex from infancy. *Exp. Brain Res.* 25, 115–130.
- Borgius, L., Restrepo, C.E., Leao, R.N., Saleh, N., and Kiehn, O. (2010). A transgenic mouse line for molecular genetic analysis of excitatory glutamatergic neurons. *Mol. Cell. Neurosci.* 45, 245–257.
- Bosch-Bouju, C., Hyland, B.I., and Parr-Brownlie, L.C. (2013). Motor thalamus integration of cortical, cerebellar and basal ganglia information: implications for normal and parkinsonian conditions. *Front. Comput. Neurosci.* 7, 163.
- Brudzynski, S.M., Wu, M., and Mogenson, G.J. (1988). Modulation of locomotor activity induced by injections of carbachol into the tegmental pedunculopontine nucleus and adjacent areas in the rat. *Brain Res.* 451, 119–125.
- Chevalier, G., Vacher, S., and Deniau, J.M. (1984). Inhibitory nigral influence on tectospinal neurons, a possible implication of basal ganglia in orienting behavior. *Exp. Brain Res.* 53, 320–326.
- Cui, G., Jun, S.B., Jin, X., Pham, M.D., Vogel, S.S., Lovinger, D.M., and Costa, R.M. (2013). Concurrent activation of striatal direct and indirect pathways during action initiation. *Nature* 494, 238–242.
- DeLong, M.R. (1990). Primate models of movement disorders of basal ganglia origin. *Trends Neurosci.* 13, 281–285.
- Ehrich, J.M., Phillips, P.E., and Chavkin, C. (2014). Kappa opioid receptor activation potentiates the cocaine-induced increase in evoked dopamine release recorded *in vivo* in the mouse nucleus accumbens. *Neuropsychopharmacology* 39, 3036–3048.
- Freeze, B.S., Kravitz, A.V., Hammack, N., Berke, J.D., and Kreitzer, A.C. (2013). Control of basal ganglia output by direct and indirect pathway projection neurons. *J. Neurosci.* 33, 18531–18539.
- Garcia-Rill, E. (1986). The basal ganglia and the locomotor regions. *Brain Res.* 396, 47–63.
- Garcia-Rill, E., Skinner, R.D., Conrad, C., Mosley, D., and Campbell, C. (1986). Projections of the mesencephalic locomotor region in the rat. *Brain Res. Bull.* 17, 33–40.
- Garcia-Rill, E., Skinner, R.D., Miyazato, H., and Homma, Y. (2001). Pedunculopontine stimulation induces prolonged activation of pontine reticular neurons. *Neuroscience* 104, 455–465.
- Giber, K., Diana, M.A., Plattner, V.M., Dugué, G.P., Bokor, H., Rousseau, C.V., Maglóczky, Z., Havas, L., Hangya, B., Wildner, H., et al. (2015). A subcortical inhibitory signal for behavioral arrest in the thalamus. *Nat. Neurosci.* 18, 562–568.
- Girard, B., and Berthoz, A. (2005). From brainstem to cortex: computational models of saccade generation circuitry. *Prog. Neurobiol.* 77, 215–251.
- Goldberg, J.H., Farries, M.A., and Fee, M.S. (2013). Basal ganglia output to the thalamus: still a paradox. *Trends Neurosci.* 36, 695–705.
- Grace, A.A. (2010). Dopamine system dysregulation by the ventral subiculum as the common pathophysiological basis for schizophrenia psychosis, psychostimulant abuse, and stress. *Neurotox. Res.* 18, 367–376.
- Grillner, S., Hellgren, J., Ménard, A., Saitoh, K., and Wikström, M.A. (2005). Mechanisms for selection of basic motor programs—roles for the striatum and pallidum. *Trends Neurosci.* 28, 364–370.
- Grillner, S., Wallén, P., Saitoh, K., Kozlov, A., and Robertson, B. (2008). Neural bases of goal-directed locomotion in vertebrates—an overview. *Brain Res. Brain Res. Rev.* 57, 2–12.
- Hikosaka, O., and Wurtz, R.H. (1983). Visual and oculomotor functions of monkey substantia nigra pars reticulata. IV. Relation of substantia nigra to superior colliculus. *J. Neurophysiol.* 49, 1285–1301.
- Hikosaka, O., Takikawa, Y., and Kawagoe, R. (2000). Role of the basal ganglia in the control of purposive saccadic eye movements. *Physiol. Rev.* 80, 953–978.
- Hikosaka, O., Nakamura, K., and Nakahara, H. (2006). Basal ganglia orient eyes to reward. *J. Neurophysiol.* 95, 567–584.
- Kravitz, A.V., Freeze, B.S., Parker, P.R., Kay, K., Thwin, M.T., Deisseroth, K., and Kreitzer, A.C. (2010). Regulation of parkinsonian motor behaviours by optogenetic control of basal ganglia circuitry. *Nature* 466, 622–626.
- Kreitzer, A.C., and Malenka, R.C. (2008). Striatal plasticity and basal ganglia circuit function. *Neuron* 60, 543–554.
- LeDoux, J.E. (2000). Emotion circuits in the brain. *Annu. Rev. Neurosci.* 23, 155–184.
- Lee, A.M., Hoy, J.L., Bonci, A., Wilbrecht, L., Stryker, M.P., and Niell, C.M. (2014). Identification of a brainstem circuit regulating visual cortical state in parallel with locomotion. *Neuron* 83, 455–466.
- Mamiya, K., Bay, K., Skinner, R.D., and Garcia-Rill, E. (2005). Induction of long-lasting depolarization in medioventral medulla neurons by cholinergic input from the pedunculopontine nucleus. *J. Appl. Physiol.* 99, 1127–1137.
- Martinez-Gonzalez, C., Bolam, J.P., and Mena-Segovia, J. (2011). Topographical organization of the pedunculopontine nucleus. *Front. Neuroanat.* 5, 22.

- Martinez-Gonzalez, C., van Andel, J., Bolam, J.P., and Mena-Segovia, J. (2014). Divergent motor projections from the pedunculopontine nucleus are differentially regulated in Parkinsonism. *Brain Struct. Funct.* 219, 1451–1462.
- Mena-Segovia, J., Bolam, J.P., and Magill, P.J. (2004). Pedunculopontine nucleus and basal ganglia: distant relatives or part of the same family? *Trends Neurosci.* 27, 585–588.
- Mena-Segovia, J., Sims, H.M., Magill, P.J., and Bolam, J.P. (2008). Cholinergic brainstem neurons modulate cortical gamma activity during slow oscillations. *J. Physiol.* 586, 2947–2960.
- Mitani, A., Ito, K., Hallanger, A.E., Wainer, B.H., Kataoka, K., and McCarley, R.W. (1988). Cholinergic projections from the laterodorsal and pedunculopontine tegmental nuclei to the pontine gigantocellular tegmental field in the cat. *Brain Res.* 451, 397–402.
- Niell, C.M., and Stryker, M.P. (2010). Modulation of visual responses by behavioral state in mouse visual cortex. *Neuron* 65, 472–479.
- Noga, B.R., Kettler, J., and Jordan, L.M. (1988). Locomotion produced in mesencephalic cats by injections of putative transmitter substances and antagonists into the medial reticular formation and the pontomedullary locomotor strip. *J. Neurosci.* 8, 2074–2086.
- Norton, A.B., Jo, Y.S., Clark, E.W., Taylor, C.A., and Mizumori, S.J. (2011). Independent neural coding of reward and movement by pedunculopontine tegmental nucleus neurons in freely navigating rats. *Eur. J. Neurosci.* 33, 1885–1896.
- Oldenburg, I.A., and Sabatini, B.L. (2015). Antagonistic but Not Symmetric Regulation of Primary Motor Cortex by Basal Ganglia Direct and Indirect Pathways. *Neuron* 86, 1174–1181.
- Orlovsky, G.N., Deliagina, T., and Grillner, S. (1999). *Neuronal Control of Locomotion: From Mollusc to Man.* (Oxford University Press).
- Perkins, E., May, P.J., and Warren, S. (2014). Feed-forward and feedback projections of midbrain reticular formation neurons in the cat. *Front. Neuroanat.* 7, 55.
- Redgrave, P., Mitchell, I.J., and Dean, P. (1987). Descending projections from the superior colliculus in rat: a study using orthograde transport of wheatgerm-agglutinin conjugated horseradish peroxidase. *Exp. Brain Res.* 68, 147–167.
- Ryczko, D., and Dubuc, R. (2013). The multifunctional mesencephalic locomotor region. *Curr. Pharm. Des.* 19, 4448–4470.
- Rye, D.B., Lee, H.J., Saper, C.B., and Wainer, B.H. (1988). Medullary and spinal efferents of the pedunculopontine tegmental nucleus and adjacent mesopontine tegmentum in the rat. *J. Comp. Neurol.* 269, 315–341.
- Saper, C.B., Swanson, L.W., and Cowan, W.M. (1979). An autoradiographic study of the efferent connections of the lateral hypothalamic area in the rat. *J. Comp. Neurol.* 183, 689–706.
- Schiller, P.H., and Stryker, M. (1972). Single-unit recording and stimulation in superior colliculus of the alert rhesus monkey. *J. Neurophysiol.* 35, 915–924.
- Shang, C., Liu, Z., Chen, Z., Shi, Y., Wang, Q., Liu, S., Li, D., and Cao, P. (2015). BRAIN CIRCUITS. A parvalbumin-positive excitatory visual pathway to trigger fear responses in mice. *Science* 348, 1472–1477.
- Sherman, D., Fuller, P.M., Marcus, J., Yu, J., Zhang, P., Chamberlin, N.L., Saper, C.B., and Lu, J. (2015). Anatomical Location of the Mesencephalic Locomotor Region and Its Possible Role in Locomotion, Posture, Cataplexy, and Parkinsonism. *Front. Neurol.* 6, 140.
- Shik, M.L., Orlovskii, G.N., and Severin, F.V. (1966a). [Organization of locomotor synergism]. *Biofizika* 11, 879–886.
- Shik, M.L., Severin, F.V., and Orlovskii, G.N. (1966b). [Control of walking and running by means of electric stimulation of the midbrain]. *Biofizika* 11, 659–666.
- Sinnamon, H.M., Ginzburg, R.N., and Kurose, G.A. (1987). Midbrain stimulation in the anesthetized rat: direct locomotor effects and modulation of locomotion produced by hypothalamic stimulation. *Neuroscience* 20, 695–707.
- Skinner, R.D., Kinjo, N., Ishikawa, Y., Biedermann, J.A., and Garcia-Rill, E. (1990). Locomotor projections from the pedunculopontine nucleus to the medioventral medulla. *Neuroreport* 1, 207–210.
- Smetana, R., Juvvin, L., Dubuc, R., and Alford, S. (2010). A parallel cholinergic brainstem pathway for enhancing locomotor drive. *Nat. Neurosci.* 13, 731–738.
- Takakusaki, K., Shiroyama, T., Yamamoto, T., and Kitai, S.T. (1996). Cholinergic and noncholinergic tegmental pedunculopontine projection neurons in rats revealed by intracellular labeling. *J. Comp. Neurol.* 371, 345–361.
- Thankachan, S., Fuller, P.M., and Lu, J. (2012). Movement- and behavioral state-dependent activity of pontine reticulospinal neurons. *Neuroscience* 221, 125–139.
- Thompson, J.A., and Felsen, G. (2013). Activity in mouse pedunculopontine tegmental nucleus reflects action and outcome in a decision-making task. *J. Neurophysiol.* 110, 2817–2829.
- Van Dort, C.J., Zachs, D.P., Kenny, J.D., Zheng, S., Goldblum, R.R., Gelwan, N.A., Ramos, D.M., Nolan, M.A., Wang, K., Weng, F.J., et al. (2015). Optogenetic activation of cholinergic neurons in the PPT or LDT induces REM sleep. *Proc. Natl. Acad. Sci. USA* 112, 584–589.
- Wall, N.R., De La Parra, M., Callaway, E.M., and Kreitzer, A.C. (2013). Differential innervation of direct- and indirect-pathway striatal projection neurons. *Neuron* 79, 347–360.
- Whelan, P.J. (1996). Control of locomotion in the decerebrate cat. *Prog. Neurobiol.* 49, 481–515.
- Zhao, S., Ting, J.T., Atallah, H.E., Qiu, L., Tan, J., Gloss, B., Augustine, G.J., Deisseroth, K., Luo, M., Graybiel, A.M., and Feng, G. (2011). Cell type-specific channelrhodopsin-2 transgenic mice for optogenetic dissection of neural circuitry function. *Nat. Methods* 8, 745–752.

Supplemental Figures

Cell

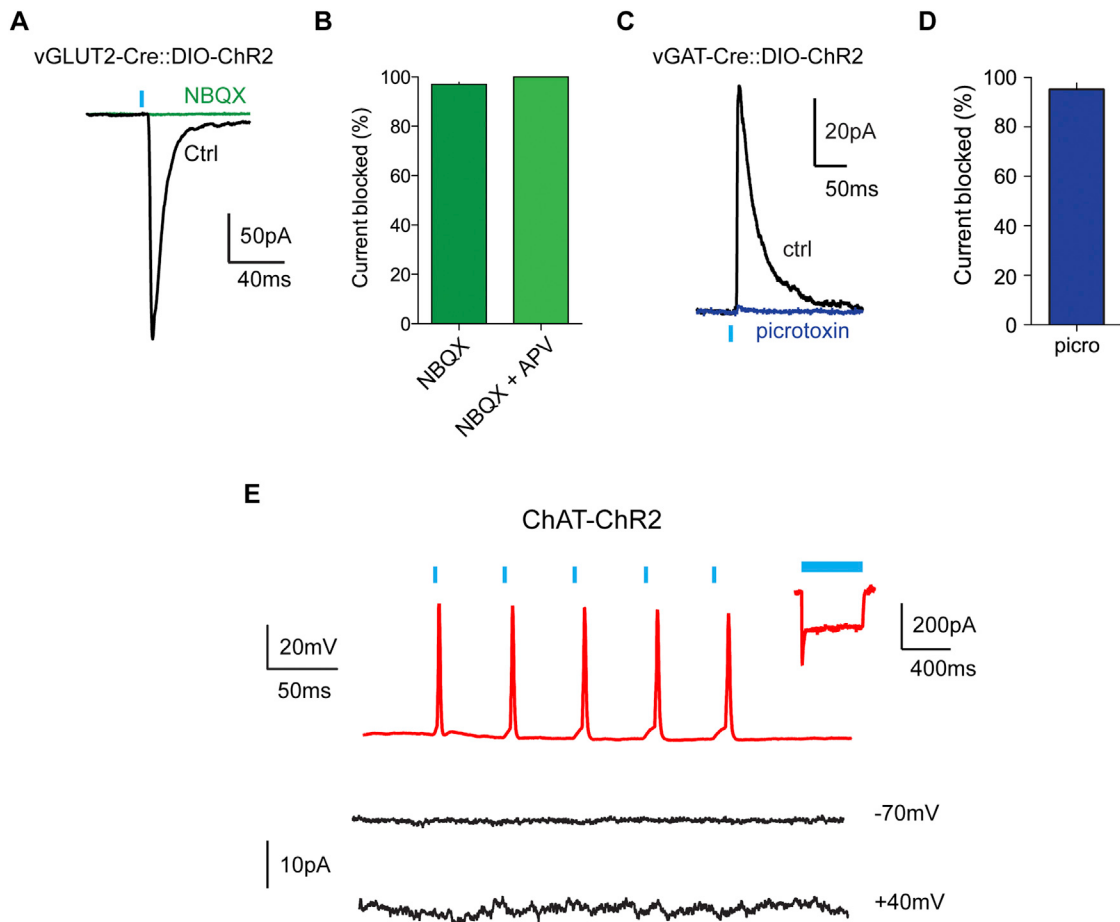


Figure S1. Confirmation of Glutamatergic, GABAergic, and Lack of Cholinergic Neurotransmission, Related to Figure 2

- (A) Example traces of light evoked EPSCs in the MLR of a vGLUT2-Cre::DIO-ChR2 mouse prior to (black) and after (red) bath application of NBQX.
- (B) Summary of bath application of NBQX and NBQX + APV. $97.5\% \pm 1.2\%$ was blocked with NBQX ($n = 4$ cells) while $100\% \pm 0\%$ was blocked with NBQX + APV ($n = 5$ cells).
- (C) Example traces of light evoked IPSCs in the MLR of a vGAT-Cre::DIO-ChR2 mouse prior to (black) and after (red) bath application of picrotoxin.
- (D) Summary of IPSC block by picrotoxin. Picrotoxin blocked $96.3\% \pm 1.9\%$ of IPSCs ($n = 4$ cells).
- (E) Top, example current clamp trace of a ChR2-positive cell responding to light stimulation at 20Hz. Inset, example voltage clamp trace during 500 ms of light stimulation of the cell. No EPSCs (middle trace, example cell held at -70 mV, 6 cells from 2 mice) or IPSCs (bottom trace, example cell held at $+40$ mV, 4 cells from the same 2 mice) were observed during light stimulation in ChR2-negative cells within the MLR.

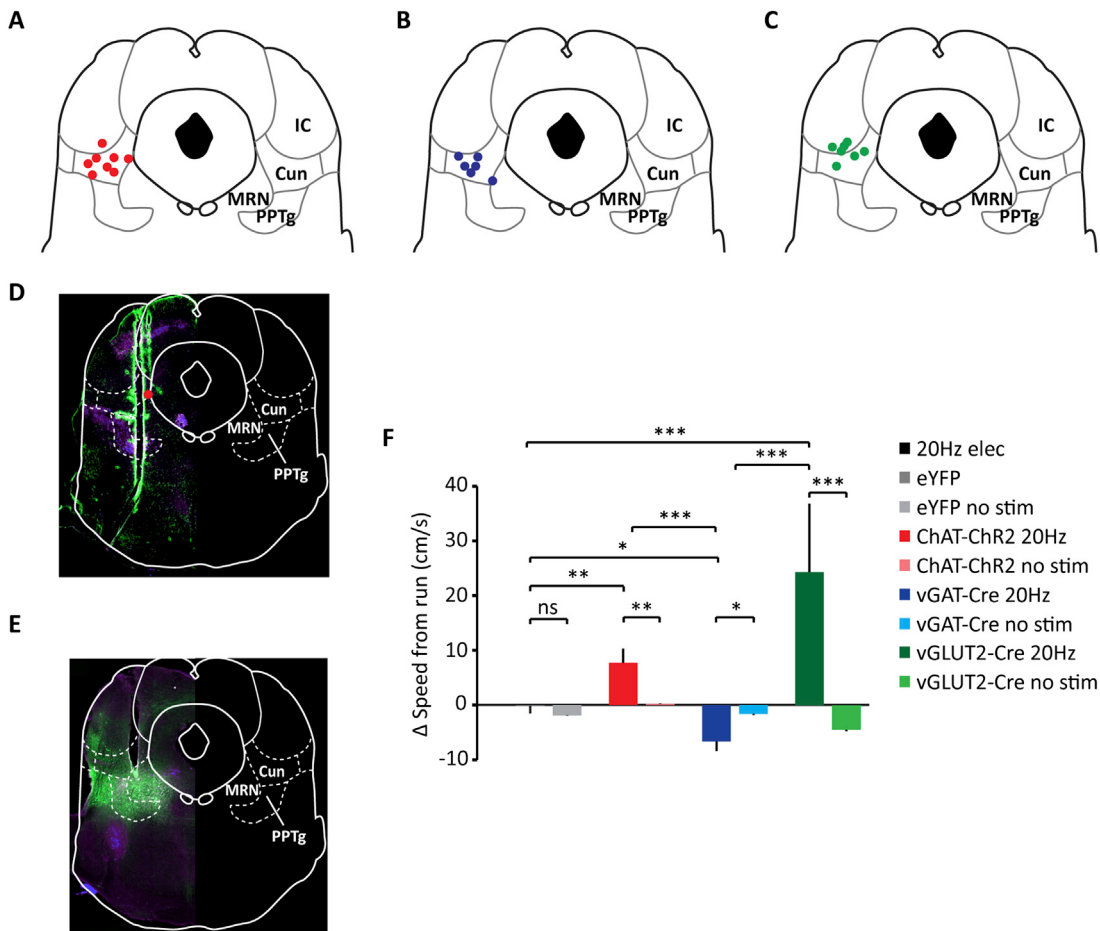


Figure S2. Example Viral Injections, Fiber and Electrode Placements, and Summary Locomotor Data, Related to Figure 2

(A–C), fiber placements for ChAT-ChR2 (A), vGAT-Cre::DIO-ChR2 (B) and vGLUT2-Cre::DIO-ChR2 mice (C).

(D) Representative image of electrode track. Some animals were stimulated with the fiber attached to the electrode for behavior data. Fiber placement along the dorsal-ventral axis was calculated by locating the lowest electrode point along the axis and extrapolating back using the noted depth from brain surface and the fiber's distance from the electrode tip (see methods for further explanation). This fiber tip stimulation point is marked with a red dot.

(E) Representative image of fiber track.

(F) Population summary for changes in speed between 2 and 5 s after onset of stimulation. Solid colors, stim; light colors, no stim. All stimulations except eYFP controls resulted in a significant change in velocity compared to baseline and no stim (lowest comparisons in graph, * $p < 0.05$, ** $p < 0.01$, *** $p < 0.001$, Wilcoxon rank sum). In addition all stimulations were significantly different from eYFP controls and the majority were different from each other (* $p < 0.05$, ** $p < 0.01$, *** $p < 0.001$ Kruskal-Wallis one-way ANOVA, $\chi^2_{3,76} = 26.41$, $p < 10^{-5}$, with Dunn-Sidak post test).

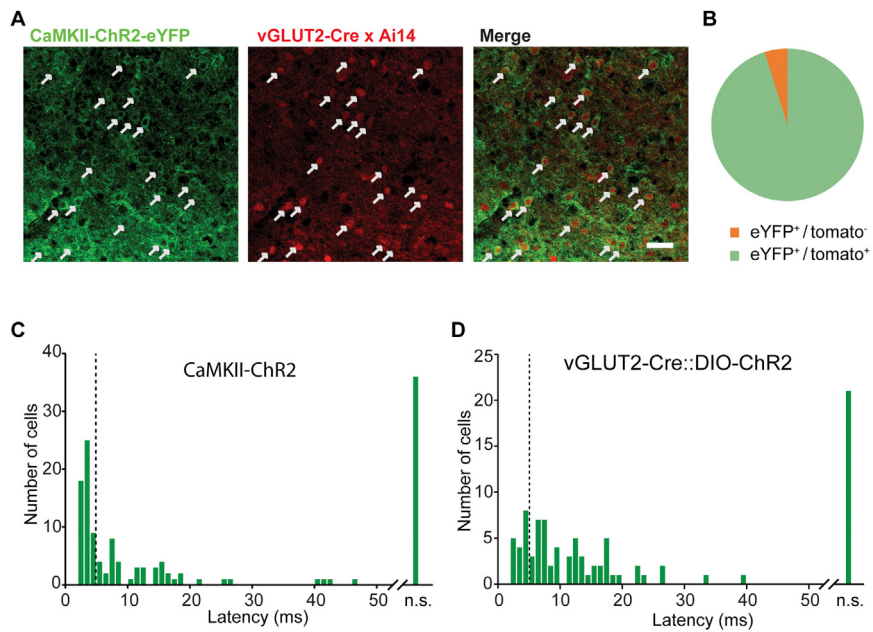


Figure S3. CaMKII α Expression Confirmation and Light Activation Latencies for CaMKII α and vGLUT2 Mice, Related to Figures 3, 4, and 6

(A) Confocal images of CaMKII α -ChR2-eYFP in a vGLUT2-Cre mouse crossed with an Ai14-tdtomato reporter. Left, cells expressing ChR2-eYFP display ringed patterns of expression; middle, tomato positive cells; right, merged images. White arrows show cells expressing both fluorophores. Scale bar 100 μ m.

(B) Pie chart showing level of specificity.

(C) Latency to significant (99% confidence interval) activation after onset of 10ms light pulse during cell ID sessions for CaMKII α -infected cells. Dotted line indicates 5ms cutoff point for labeled classification ($n = 132$ cells from 8 mice).

(D) Same as (C) but in vGLUT2-Cre::DIO-ChR2 mice ($n = 91$ neurons from 6 mice).

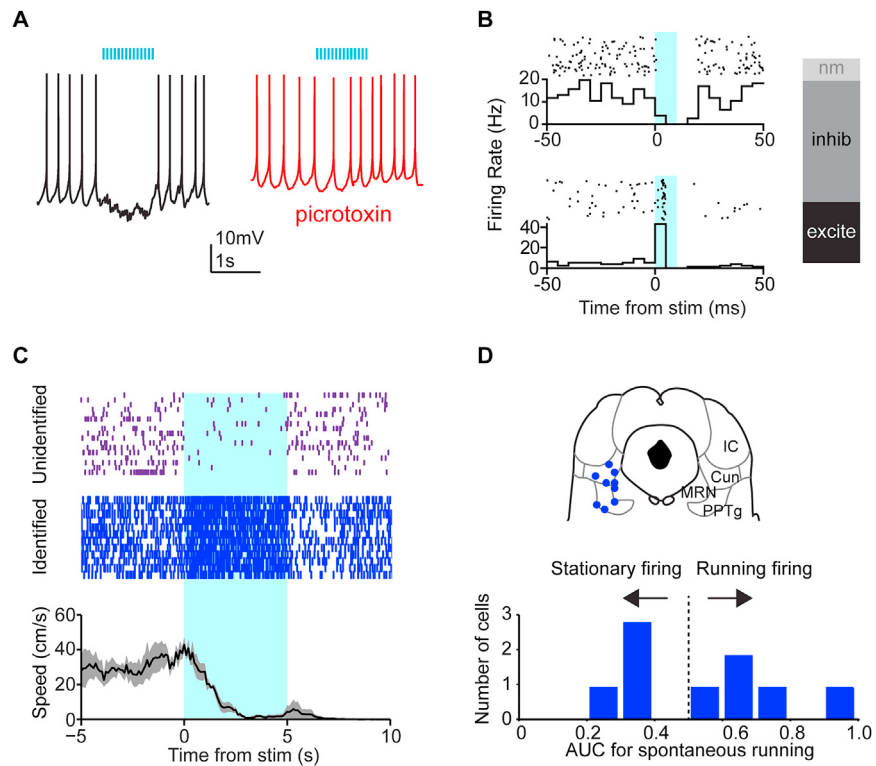


Figure S4. Characterization of MLR GABAergic Inhibition and Locomotor Activity, Related to Figures 2, 3, and 4

(A) Current clamp traces showing inhibition of spiking responses in a ChR2-eYFP negative cell within the MLR in response to 20Hz GABAergic stimulation (left, black trace). Inhibition was blocked with bath-applied picrotoxin (right, red trace).

(B) Top, raster and PSTH of an unidentified neuron suppressed during 10 ms pulses (bottom). Right, fractions of excited (excite), inhibited (inhib), or non-modulated (nm) units during the 10 ms pulse (19 excited, 38 inhibited, 7 non-modulated from 4 mice).

(C) Top and middle, example rasters of an unidentified neuron and an identified GABAergic neuron, respectively, aligned to 5 s, 20Hz stimulation. Bottom, speed of the mouse aligned to stimulation onset when running.

(D) Top, recording sites of identified GABAergic neurons. Bottom, AUCs from ROC analysis for the identified GABAergic population. All AUCs were significant (Lag test, Methods).

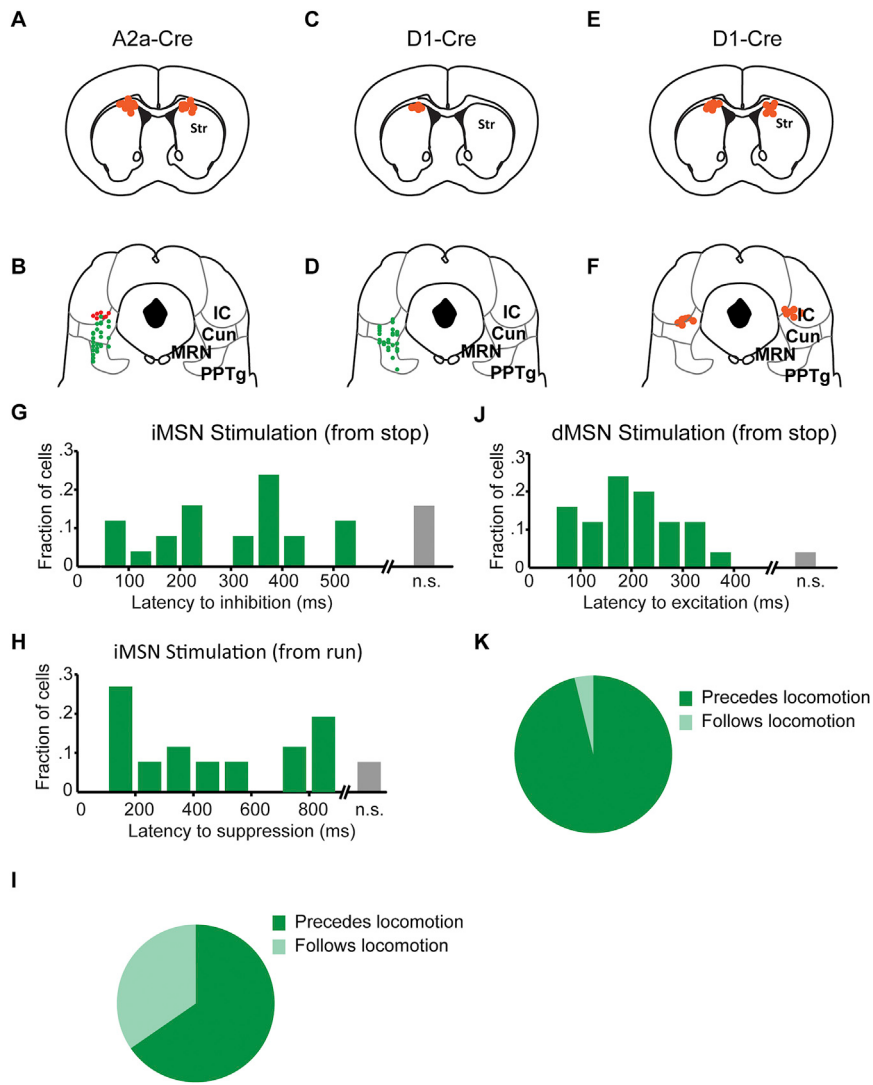


Figure S5. Electrode, Fiber Placements, and Histograms of Latency to Excitation or Suppression of MLR Glutamatergic Neurons in Response to dMSN or iMSN Stimulation, Related to Figure 6

- (A) Optical fiber tip placements in striatum for stimulation of iMSNs (Figures 6E and 6F).
- (B) Recording site locations (green) for iMSN stimulation experiments. Optical fiber placements (red) are for behavior only (Figures 6G and 6H) as the fiber tip moved with the electrode between recording sites.
- (C) Optical fiber tip placements in striatum for stimulation of dMSNs during recording of identified neurons in the MLR (Figures 6A and 6B).
- (D) Recording site locations for the same experiments.
- (E) Optical fiber tip placements in striatum for stimulation of dMSNs while inhibiting CaMKII α -eNpHR3.0 cells in the MLR (Figures 6C and 6D).
- (F) Optical fiber tip placements for MLR inhibition in the same experiments.
- (G) Histogram of latencies to significant inhibition following iMSN stimulation onset from the stationary condition.
- (H) Histogram of latencies to significant inhibition following iMSN stimulation onset from running.
- (I) Pie chart separating the number of neurons inhibited prior to the offset of locomotion due to iMSN stimulation.
- (J) Histogram of latencies to significant excitation following dMSN stimulation onset from the stationary condition.
- (K) Pie chart separating the number of neurons excited prior to the onset of locomotion due to dMSN stimulation.

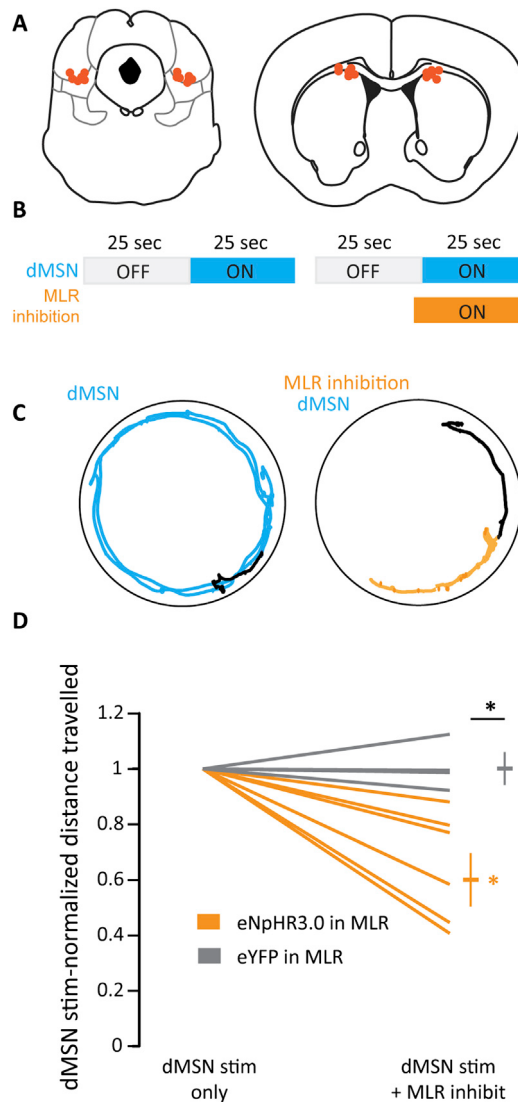


Figure S6. Inhibiting Glutamatergic Cells in the MLR Attenuates the Locomotor Effects of dMSN Stimulation in the Open Field, Related to Figure 6

(A) Fiber tip placement in the MLR (left) and striatum (right).

(B) Experimental time course.

(C) Example traces in the open field. Left, trajectory of the mouse during bilateral dMSN stimulation only (blue line, 1-2mW continuous light). Right, trajectory during dMSN stimulation while inhibiting glutamatergic cells in the MLR (orange line, 10mW continuous green light in the MLR). Black lines indicate trajectory during baseline periods.

(D) Summary of stimulation effects normalized to dMSN stimulation only (eNpHR3.0, n = 6 mice; eYFP n = 4 mice; * $p < 0.05$, Wilcoxon rank sum between groups and sign rank within group).

Cell

Supplemental Information

Cell-Type-Specific Control of Brainstem

Locomotor Circuits by Basal Ganglia

Thomas K. Roseberry, A. Moses Lee, Arnaud L. Lalive, Linda Wilbrecht, Antonello Bonci, and Anatol C. Kreitzer

Supplemental Experimental Procedures

Animals and stereotactic surgery

86 adult transgenic or wild-type mice on a C57BL/6 background aged 50 to 100 days were used in the experiments. 13 wild-type mice (8 males, 6 females) were used for electrical stimulation experiments (Fig. 1). 10 vGLUT2-ires-Cre (3 females, 7 males, Jackson Stock# 016963, Fig. 1, 2, S3), 9 vGAT-ires-Cre (4 females, 5 males, Jackson Stock# 016962, Fig. 1, S5), 6 ChAT-ChR2 (2 females, 4 males, Jackson Stock# 014546, Fig. 1) and 6 wild-type C57BL/6 (2 females, 4 males, Jackson Stock# 000664, Fig. 2) mice were used for optogenetic stimulation, inhibition or recording experiments. 6 vGLUT2-Cre and 5 vGAT-Cre (4 and 2 males and 2 and 3 females respectively, same Jackson stock) were used for rabies tracing experiments (Fig. 3). 18 D1-Cre mice (8 females, 10 males, GENSAT #030778-UCD) were used for dMSN stimulation while recording identified responses from unidentified or identified glutamatergic neurons or inhibiting the MLR (Fig. 4). 12 A2a-Cre mice (8 males, 4 females, GENSAT #031168-UCD) were used for iMSN stimulation while recording responses from unidentified or identified glutamatergic neurons or stimulating the MLR (Fig. 4). 2 male vGLUT2-Cre mice crossed into an Ai14 line (Jackson Stock #007914) were used for confirmation of CAMKII α expression in vGLUT2-expressing neurons (Fig. S3). 2 male vGAT-Cre mice, 2 vGLUT2-Cre and 2 ChAT-ChR2 mice, all males, were used in slice experiments (Fig. S2 and S5). No randomization of animals was implemented and the researchers were not blinded.

All procedures were in accordance with protocols approved by the UCSF Institutional Animal Care and Use Committee. Mice were maintained on a 12/12 light/dark cycle and fed *ad libitum*. Experiments were carried out during the dark cycle. All surgeries were carried out in aseptic conditions while mice were anaesthetized with isoflurane (5% for induction, 0.5-1.5% afterward) in a manual stereotactic frame (Kopf). Buprenorphine HCl (0.1 mg kg⁻¹, intraperitoneal injection) and Ketoprofen (5 mg kg⁻¹, subcutaneous injection) was used for postoperative analgesia. Mice were allowed to recover for five to seven days after surgeries before habituation to the trackball.

Viral injection

For cell-type-specific viral infection of MLR neurons, we injected 300 to 500 nL of adeno-associated virus serotype 5 (AAV5) carrying channelrhodopsin 2.0 (ChR2) fused to enhanced yellow fluorescent protein (eYFP) in a double-floxed inverted open reading frame (DIO) under the control of the EF1 α promoter (AAV5-EF1 α -DIO-ChR2-eYFP for DIO-ChR2; all viruses obtained from UNC Vector Core or University of Pennsylvania Vector Core), AAV5-EF1 α -DIO-eYFP for controls (Fig. 1 & 2). For inhibition of glutamatergic neurons in the MLR, we injected AAV expressing halorhodopsin (eNpHR3.0) expressed under the CAMKII α promoter (AAV5-CAMKII α -eNpHR3.0-eYFP) (Fig. 2 & Fig. 4). MLR injections were made bilaterally at -0.80 mm anteroposterior (AP) measured from Lambda, \pm 1.2 mm mediolateral (ML) and -3.6 dorsoventral (DV) measured from the skull surface (5 μ L NanoFil with 33ga Needles; WPI) mounted to a microsyringe pump (UMP3; WPI) and controller (Micro4; WPI). Injection speed was 100 nL min $^{-1}$ and the injection needle was raised 7 minutes after completion. For activation of the striatal dMSN or iMSN population (Fig. 6 & Fig. S6) we injected 1.000 μ L at 200 nL min $^{-1}$ bilaterally at +0.8 mm AP from Bregma, \pm 1.5 mm ML and -2.5 DV from the brain surface. MLR infection for these experiments was carried out at the same coordinates for the MLR as above but using ChR2 expressed under the CAMKII α promoter (AAV5-CAMKII α -ChR2-eYFP) for stimulation, or halorhodopsin (eNpHR3.0) for inhibition (AAV5-CAMKII α -eNpHR3.0-eYFP). ChR2 viruses were allowed to express for 3 to 5 weeks before experiments while eNpHR3.0 viruses were allowed to express for 6 to 8 weeks.

For characterization of inputs to specific MLR populations using rabies tracing, vGLUT2-ires-Cre or vGAT-ires-Cre mice were injected in the MLR (coordinates above) with a mixture of DIO-TVA-mcherry (AAV5-EF1a-FLEX-mCherry; “TVA”) and rabies glycoprotein (AAV5-CAG-FLEX-RG, “RG”) (Salk Institute) . On Day 14, mice were injected with EnvA-pseudotyped G-deleted rabies-eYFP, which only infects cells expressing the TVA receptor (Wall et al., 2010) . Tissue was fixed for analysis at Day 23.

Surgical Preparation

For all experiments, mice were implanted with a custom stainless steel headbar for head fixation. The scalp was removed and skull scraped clean and dry using a scalpel. Cyanoacrylate glue (Vetbond, 3M) was lightly dabbed on the skull and a base of dental acrylic (Ortho Jet; Lang Dental) applied in a circle around Lambda to provide the skull/headbar interface. The headbar was further cemented with dental acrylic, and the central hole was then filled with silicone elastomer (Kwik-Cast; WPI).

For activation of striatal MSNs while either recording or stimulating in the MLR (Fig. 6, Fig. S6), 200- μ m-diameter optical fibers (Thorlabs #FT200UMT) were: (1) glued into 1.25 mm ferrules (Thorlabs CFLC128-10), (2) polished, and (3) implanted bilaterally 0.5 mm above the striatal viral injection site after headbar mounting by drilling a 0.5 mm hole in the skull, lowering the fiber over 1 minute and gluing into place with Vetbond followed by dental acrylic. For eNpHR3.0 experiments (Fig. 6, Fig. S6), a second set of fibers with ferrules was implanted 0.5 mm over the MLR viral injection site. Mice were allowed 7 to 10 days of recovery from surgery.

For neural recording and some stimulation experiments, a 0.5 to 1 mm burr hole was drilled at \pm 1.2 mm mediolateral and -0.8 anterodorsal from lambda. The head plate was filled with silicone elastomer and the animal was allowed to recover for at least 3-4 hours. The animal was then placed on the trackball and the silicone plug removed.

Behavior

Mice were habituated to the trackball for 2 to 3 days prior to the experiment. Movement of the trackball was monitored by 2 optical mice fed into custom MATLAB software as described in Neill and Stryker, 2010 (Lee et al., 2014). For electrical stimulation experiments, a concentric bipolar stimulating electrode (FHC part no CBBBE75) was lowered into the brainstem and 200 μ A, 200 μ s electric current delivered at 20 Hz for 5 seconds with 20-40 seconds between trials. For optical stimulation experiments, blue light was passed through a 200 μ m fiber attached to a recording probe (described below) using a 473 nm laser (OEM, part no 10010351) coupled to an optical multimode fibre (200 μ m, 0.39 NA FC/PC, Thorlabs part no M83L01). This allowed these mice to also be used in optical tagging experiments. Light

was delivered in 10 ms pulses at 20 Hz trains of 5 second duration with 20 to 40 seconds between trains at 5 to 10 mW.

For dMSN stimulation followed by MLR inhibition (Fig. 4), 10 seconds of 2.5 mW blue light was delivered unilaterally (side randomized) into a striatal ferrule. At 5 seconds into stimulation, green light (OEM laser, part no G00003) was delivered for 5 seconds continuously at 10 mW bilaterally to the MLR. 5 to 6 minutes were allowed between stimulations. For the open field version of the experiment (Fig. S6), green light in the MLR was delivered 5 seconds before the blue light in the striatum and both were on continuously for 30 seconds, with 5 minutes between stimulations. A 25 second window prior to stimulation was used as the baseline for locomotion and a 25 second window beginning 5 seconds after striatal stimulation onset was used for analyzing locomotion during stimulation. Locomotion was tracked and calculated using ETHOVISION 7.1 hardware and software using parameters described previously (Freeze et al., 2013). For both head-fixed and freely-moving experiments, no inhibition trials (in which the green laser was omitted) were interleaved with inhibition trials.

For iMSN stimulation followed by MLR stimulation (Fig. 4), 10 seconds of 2.5 mW blue light was delivered bilaterally into the striatal ferrules. At 5 seconds after onset of striatal stimulation, 10 ms pulses of blue light were delivered at 20 Hz trains for 5 seconds, with power (at fiber tip) set at 5-10 mW. Trials with no MLR stimulation were interleaved with stimulation trials. If an animal did not run with MLR stimulation alone, it was excluded (3 mice total).

For recording activity during spontaneous locomotion in vGLUT2-Cre::DIO-ChR2 mice (Fig. 2), 2 light-active identification sessions were carried out before and after (“Light Evoked”; Fig. 2) a locomotor session (“Spontaneous”; Fig. 2) in which mice were allowed to run freely on the trackball for 15 to 20 minutes.

For recording MLR activity during iMSN or dMSN stimulation, 2 optical identification sessions were carried out before and after an MSN stimulation session. During the stimulation session, blue light was delivered bilaterally (iMSN) or unilaterally (dMSN) at 2.5 mW for 5 sec with 20 to 60 seconds between stimulations.

In Vivo Electrophysiology

Extracellular spikes were recorded using NeuroNexus silicon probes (part no A1x16-10mm-100-177-A16). 200- μ m-diameter optical fibers were manually mounted on the probe, with the upper-most recording site approximately 100 μ m below the tip of the fiber and 200 μ m lateral from the probe surface. This setup greatly reduced optical artifact. Once the probe had been lowered in the brain, a drop of agarose was used to stabilize it. Voltage signals were band-pass filtered between 150 and 8000 Hz. Each data stream was amplified, processed and digitally captured using commercial hardware and software (Plexon). Typically, only 1 unit was identifiable per recording depth. After each recording, the probe was driven 100 to 200 μ m to find other cells. Neurons that appeared to stay on the same channel or appeared on a channel just above a site that had a light-active neuron during the previous recording were excluded.

Optical Identification of ChR2-Expressing Neurons

At the beginning of each experiment involving identified ChR2-expressing neurons (Fig. 2, 4, S5), the probe was lowered to the presumed depth of the MLR through the burr hole and allowed to settle for 10 to 45 minutes. The fiber attached to the probe was coupled to a 473 nm laser (OEM, part no 10010351) using an optical multimode fibre (200 μ m, 0.39 NA FC/PC, Thorlabs part no M83L01). Once a stable recording was established, blue light was flashed for 10 ms at 2 to 10 mW through the fiber into the brain at 1-2 Hz for 200 to 300 repetitions. Laser power was adjusted to minimize the latency of activation while also minimizing optical artifact. Once a neuron was identified as possibly being light active, the locomotor/stimulation session would proceed after which a post identification session would be carried out to ensure another unit had not moved into the recording space. Final clustering was performed post hoc.

Analysis of Neural and Behavioral Data

Pre- and post-identification sessions were merged with the associated locomotor or stimulation session to sort single units on the same principle component and peak-to-trough amplitude spaces. Single units were sorted using Offline sorter V2.1 (Plexon). Recorded units in which more than 1% of interspike intervals were shorter than 2 ms were excluded from analysis. MANOVA ($p < 0.01$) and J3 (> 3.0) parameters in 3 dimensions were used to ensure cluster quality.

Light responses were determined using 1 ms bins in NeuroExplorer V4.133. All other analysis of neural and behavioral data was carried out using custom MATLAB software which is available upon request. A neuron was considered identified (ChR2-positive) if: (1) its firing rate cleared the 99% confidence interval (based on a 20 ms baseline period prior to stim) within 5 ms after the onset of the 10 ms pulse, (2) light-evoked spike waveforms (occurring within the 10 ms of the light pulse) were identical to the spontaneous waveform ($R > 0.9$), and (3) light-evoked responses displayed jitter relative to the light onset (indicating spikes were not related to a light artifact). We chose the 5 ms cutoff as there were no light responses prior to 2 ms and therefore di-synaptic activity within a <3 ms time window would be low (Fig. S3). To generate excited/inhibited/non-modulated populations for Figure S5 during GABAergic identification, excited neurons were classified as having multiple bins above the 99% confidence interval during the 10ms pulses (therefore excited neurons could be classified as excited but not identified), inhibited neurons were classified as having multiple bins below the 99% confidence interval and non-modulated fell into neither category. Neural and locomotor data was binned in 100 ms (vGLUT2-Cre::DIO-ChR2, A2a-Cre::CAMKII α -ChR2, D1-Cre::CAMKII α -eNpHR3.0) or 50 ms (D1-Cre::DIO-ChR2) windows for ROC analysis which was carried out as described in Freeze et al. 2013 (Freeze et al., 2013). To obtain a p-value, Area Under the Curve (AUC) was calculated with the speed and firing rate data lagged at all time points with greater than 10 seconds of overlapping data. A zero lag AUC outside (two-tailed) 99 % of lagged AUCs was considered significant. To calculate speed versus firing rate correlations, both locomotor and firing rate data was binned in 500 ms windows and z-scored based on firing rates when the mouse was stationary. Linear regression was run on individual cells and $p < 0.01$ using an F-test determined significant correlations. To calculate changes in firing rate aligned to starts,

data was Z-scored based on a 5 sec window of time in which the mouse was stationary before the onset of locomotion or stimulation. To calculate the probability of a start within 1 second given firing rate, data was binned in 100ms windows and z-scored based on stationary firing rates. For spontaneous locomotion aligned to start onset or dMSN stimulation, only trials in which the mouse was stationary ($<1 \text{ cm s}^{-1}$) were used. For iMSN stimulation, only trials in which the mouse was moving between 5 and 20 cm s^{-1} were used. For both conditions, data was binned in 100 ms windows and z-scored based on the 5 sec baseline. For MLR stimulation data, trials in which the mouse moved $<1 \text{ cm s}^{-1}$ were determined to be from a stop while trials in which the mouse was traveling $>2 \text{ cm s}^{-1}$ were considered to be from a run. To quantify changes in speed from a run, the average speed for the 1 second prior to stimulation was subtracted from the average speed for the final 3 seconds of stimulation. For MLR inhibition, only trials in which the mouse was moving between 2 cm s^{-1} and 40 cm s^{-1} were used. As a control, we determined how locomotion would change spontaneously given the same baseline conditions using all data points outside of the stimulation windows with the same baseline criteria as stimulation trials. For statistics a subset of these points were randomly drawn to match sample size to compare with stimulation periods. To classify CaMKII α -identified and unidentified neurons were classified as excited, inhibited or unmodulated during dMSN or iMSN stimulation, the 5 s before stimulation onset was compared by Wilcoxon rank sum to the 5 s during stimulation using $p < 0.01$ for significance. Latency to excitation of a CaMKII α -identified MLR neuron during dMSN or iMSN stimulation (Fig. 4) was determined as the first bin that exceeded 2 standard deviations for 2 consecutive bins. Latency to inhibition was determined as the first bin that fell below 1 s.d. for 2 consecutive bins. Locomotor start onset or latency (Fig. 4) was determined by finding 1 cm s^{-1} threshold crossings and going back to the most recent local minimum within the 1 second preceding the threshold crossing. Latency to deceleration onset (Fig. 4) was defined by the first of 3 consecutive bins after stimulation in which a 5 cm s^{-2} deceleration was observed. Latency results were not significantly different using 2, 5 and 10 cm s^{-2} criteria. Data that were binomial (true or false for a population) were tested using a 1 sided binomial test. χ^2 test was used to detect differences in population

frequencies. All other data were analyzed using a Kruskal-Wallis one-way ANOVA with a Dunn-Sidak post hoc test or a Wilcoxon rank sum as noted negating the need for variance and normality estimates.

Electrophysiology in acute slices

Mice were euthanized with a lethal dose of ketamine and xylazine followed by transcardial perfusion with 8 ml of ice cold artificial corticospinal fluid (aCSF) containing (in mM): glycerol (250), KCl (2.5), MgCl₂ (2), CaCl₂ (2), NaH₂PO₄ (1.2), HEPES (10), NaHCO₃ (21) and glucose (5). Coronal slices (250uM) containing the MLR were then prepared with a vibratome (Leica) in the same solution, before incubation in 33° C aCSF containing (in mM): NaCl (125), NaHCO₃ (26), NaH₂PO₄ (1.25), KCl (2.5), MgCl₂ (1), CaCl₂ (2), glucose (12.5), continuously bubbled with 95/5% O₂/CO₂. After 30 minutes of recovery, slices were either kept at room temperature or transferred to a recording chamber superfused with recording aCSF (2.5 ml/min) at 33° C . Whole-cell current-clamp recordings were obtained using an internal solution containing (in mM): KGluconate (130), NaCl (10), MgCl₂ (2), CaCl₂ (0.16), EGTA (0.5), HEPES (10). Voltage-clamp recordings were obtained using an internal solution containing (in mM): CsMeSO₃ (120), CsCl (15), NaCl (8), EGTA (0.5), HEPES (10), Mg-ATP (2), Na-GTP (0.3), TEA-Cl (10), QX-314 (5). Spiking or synaptic release were evoked by flashing 470nm filtered LED (Prizmatix) blue light through the objective (1-10 msec pulse, 1mW/cm²). EPSCs and IPSCs were measured while holding the membrane potential at -70mV and 0mM, respectively, at 20s intervals. The MLR was identified as the region lateral to the decussation of the superior cerebellar peduncle. Picrotoxin, APV and NBQX were purchased from Tocris, prepared at stock concentration in H₂O, then diluted in aCSF for bath application. Data was acquired with custom Igor software.

Histology.

Animals were euthanized with a lethal dose of ketamine and xylazine (400 mg ketamine plus 20 mg xylazine per kilogram of body weight, i.p.) and transcardially perfused with PBS, followed by 4% paraformaldehyde (PFA). Following perfusion, brains were transferred into 4% PFA for 16 –24 h and

then moved to a 30% sucrose solution in PBS for 2–3 d (all at 4 deg C). Brains were then frozen and cut into 30 µm coronal sections with a sliding microtome (Leica Microsystems, model SM2000R) equipped with a freezing stage (Physitemp) and mounted on slides. Slides were blocked for 1 hour in 10% Normal Donkey Serum (NDS) in 0.5% PBST (1% for ChAT staining) then incubated overnight in primary antibody (1:500), 3% NDS in 0.5% PBST (1% for ChAT staining). The following day, they were washed 3 times for 10 minutes each in 0.5% PBST (1% for ChAT staining) and incubated for 1 hour in secondary antibody (1:1000), 3% NDS in 0.5% PBST (1% for ChAT staining) and 1:2000 DAPI. After this, slides were washed for 10 minutes in 0.5% PBST and 2 more 10 min periods with 1:1 PBS. Slides were then washed with 0.05% lithium carbonate and alcohol, rinsed with diH₂O, and coverslipped with Cytoseal 60.

Slides were scanned on a VS120 semi-automated fluorescent slide scanner (Olympus Scientific Solutions Americas Corp, USA). Some figure images were acquired using a 6D high throughput microscope (Nikon, USA) or SP5 confocal (Leica, USA), globally gamma-adjusted to reduce background, and pseudocolored using freely available Fiji software. Settings were constant across confocal images in Fig. 1. Confocal and wide view images in Fig. 1, 3 and S1 were made brighter for better print quality using Photoshop function “Vibrance” and “Replace Color” to change LUT. No detail was lost during this manipulation.

Rabies cell counts and injection site verification were manually acquired using open source code Fiji run on the ImageJ platform (NIH, BetheMD). Manual registration of slices was performed by extracting whole slice images using Fiji, then performing scaled rotation in Adobe Illustrator, using the Paxinos mouse atlas (Academic Press, Orlando, FL) panels as a background reference. Animals with less than 100 total neurons labelled with eYFP were excluded (n = 3 exclusions). Areas proximal to (PAG and Inferior colliculus) and within the MLR (CUN, PPTg, MRN) were excluded from fraction of total cell calculations so long range connections could be weighted fairly. Regarding the outlier in Fig. 2d, the data is significant with and without it ($p < 0.05$, Wilcoxon rank sum).

To determine the site of recording or stimulation along the dorsal-ventral axis, the lowest depth of the electrode was noted both post hoc and during the experiment. The difference between these two values was then subtracted from the noted depth during a given recording. For recordings, the recording site distance from the electrode tip was further subtracted to give a more exact position. The electrode track itself was used to locate the ML and AP position. Neurons determined to be outside of the MRN, Cun or PPTg were excluded.

Supplemental Methods References

- Freeze, B.S., Kravitz, A.V., Hammack, N., Berke, J.D., and Kreitzer, A.C. (2013). Control of basal ganglia output by direct and indirect pathway projection neurons. *The Journal of neuroscience : the official journal of the Society for Neuroscience* *33*, 18531-18539.
- Lee, A.M., Hoy, J.L., Bonci, A., Wilbrecht, L., Stryker, M.P., and Niell, C.M. (2014). Identification of a brainstem circuit regulating visual cortical state in parallel with locomotion. *Neuron* *83*, 455-466.
- Wall, N.R., Wickersham, I.R., Cetin, A., De La Parra, M., and Callaway, E.M. (2010). Monosynaptic circuit tracing *in vivo* through Cre-dependent targeting and complementation of modified rabies virus. *Proc Natl Acad Sci U S A* *107*, 21848-21853.